

PPPL-2290 (Nov. 1985)
Comp. Phys. Rep. **4**(3-4), 183-244 (Aug. 1986)

Fokker-Planck and Quasilinear Codes*

Charles F. F. Karney
Plasma Physics Laboratory, Princeton University
P.O. Box 451
Princeton, New Jersey 08544-0451, U.S.A.

Abstract

The interaction of radio-frequency waves with a plasma is described by a Fokker-Planck equation with an added quasilinear term. Methods for solving this equation on a computer are discussed.

*Presented at the 3rd European Workshop on Problems in the Numerical Modeling of Plasmas, Varenna, Italy, September 10-13, 1985. Reprinted in *Problems in the Numerical Modeling of Plasmas*, edited by K. Appert (1986).

I. Introduction

In this paper, I will concentrate on those Fokker–Planck models which are most useful for the study of rf-driven currents.¹ I will therefore take the plasma to be azimuthally symmetric about the magnetic field and homogeneous (representative of the central portion of a tokamak plasma). The Fokker–Planck equation then reduces to an equation in time and two velocity (or momentum) dimensions only. This simplified model yields a wealth of interesting physics and furthermore illustrates the main numerical problems encountered in more complicated situations. In addition to the collision term, the equation will include the effects of externally injected rf power via a quasilinear diffusion term, and a dc electric field. (The electric field arises whenever the current is time-varying, e.g., during current ramp-up.) Because the wave interacts with very fast electrons, relativistic effects are also considered. In addition, the adjoint method for solving for moments of the Fokker–Planck equation is discussed. This method allows for a great reduction (by orders of magnitude) in the amount of computer time required.

The paper is divided into three parts: In the first part of the paper, I give the formulation of the Fokker–Planck equation. In sec. II, the Fokker–Planck equation and the coordinate systems are introduced. The collision operator and approximations to it are given in secs. III and IV. Corresponding expressions for the quasilinear diffusion operator are given in sec. V. The next part of the paper describes the numerical solution of the equation. Its boundary conditions are considered in sec. VI. Sections VII and VIII describe the spatial and temporal differencing of the equation. In sec. IX, we describe techniques for obtaining the time asymptotic solution to the equation. The last part of the paper describes the incorporation of relativistic effects (sec. X) and the adjoint method for solving the Fokker–Planck equation (sec. XI).

The numerical methods presented here are those used in the Fokker–Planck code used by the author. A word about the lineage of this code is in order: Fokker–Planck codes were developed at Livermore by Killeen *et al.*^{2,3} for the study of mirror-machine plasmas. The latest stage in the development of these codes is FPPAC⁴ which is a two-dimensional multispecies nonlinear Fokker–Planck package. The Livermore code was extensively modified by Winsor and Fallon for the study of runaway electrons, which was undertaken by Kulsrud *et al.*⁵ This code has been used by the author in various studies of current drive beginning with lower hybrid current drive.⁶ Over the years several further modifications have been made, although the basic structure of the code is the same as that of Kulsrud *et al.*

The assumption of a homogeneous magnetic field is warranted in the study of rf heating and current drive in tokamaks if the rf interacts only with circulating particles. This is often not the case (for example during ion- and electron-cyclotron heating) in which case proper account should be taken of trapped particles. This has been done in so-called *bounce-averaged* codes^{7–9} in which the distribution function is averaged over the bounce motion of the trapped particles. In tokamaks this leads to a modification of the coefficients appearing in the Fokker–Planck equation but the numerical treatment of the equation is largely unaltered. In machines with more complicated particle orbits, the distribution may be a multi-valued function of the velocity coordinates. This occurs in tandem mirrors where there is more than one population of trapped particles. In this case, special techniques are required.⁹

II. Preliminaries

A. The Fokker–Planck equation

We write the Fokker–Planck equation for the electrons e as

$$\frac{\partial f_e}{\partial t} - \sum_s C(f_e, f_s) + \nabla \cdot \mathbf{S}_w + \frac{q_e \mathbf{E}}{m_e} \cdot \nabla f_e = 0, \quad (1)$$

where q_s and m_s are the charge and mass of species s , $C(f_a, f_b)$ is the collision term for species a colliding off species b , the sum extends over all the species of the plasma (typically electrons and ions),

\mathbf{S}_w is the wave (w)-induced quasilinear flux, and $\mathbf{E} = E\hat{\mathbf{v}}_{\parallel}$ is the electric field (assumed to be parallel to the magnetic field). The quantity q_s carries the sign of the charge, thus $q_e = -e$. The subscripts \parallel and \perp refer to the directions parallel and perpendicular to the magnetic field. The $\nabla \equiv \partial/\partial\mathbf{v}$ operator operates in velocity space.

Because collisions in a plasma are primarily due to small-angle scattering, the collision term can be written as the divergence of a flux

$$C(f_a, f_b) = -\nabla \cdot \mathbf{S}_c^{a/b},$$

in which case eq. (1) can be expressed as

$$\frac{\partial f_e}{\partial t} + \nabla \cdot \mathbf{S} = 0, \quad (2)$$

where

$$\mathbf{S} = \mathbf{S}_c + \mathbf{S}_w + \mathbf{S}_e$$

is the total flux in velocity space, and

$$\mathbf{S}_c = \sum_s \mathbf{S}_c^{e/s}, \quad (3)$$

$$\mathbf{S}_e = \frac{q_e \mathbf{E}}{m_e} f_e, \quad (4)$$

are the collisional (c)- and electric-field (e)-induced electron fluxes.

From eq. (2) we can derive the conservation laws

$$\frac{\partial}{\partial t} \int_V f_e d^3\mathbf{v} + \int_A \mathbf{S} \cdot d^2\mathbf{A} = 0, \quad (5a)$$

$$\frac{\partial}{\partial t} \int_V m_e \mathbf{v} f_e d^3\mathbf{v} + \int_A m_e \mathbf{v} \mathbf{S} \cdot d^2\mathbf{A} = \int_V m_e \mathbf{S} d^3\mathbf{v}, \quad (5b)$$

$$\frac{\partial}{\partial t} \int_V \frac{m_e v^2}{2} f_e d^3\mathbf{v} + \int_A \frac{m_e v^2}{2} \mathbf{S} \cdot d^2\mathbf{A} = \int_V m_e \mathbf{v} \cdot \mathbf{S} d^3\mathbf{v}, \quad (5c)$$

where V is some volume in velocity space and A is its boundary. These equations are statements of conservation of number, momentum, and energy.

Typically, two types of terms appear in \mathbf{S} : a diffusion term and a friction term

$$\mathbf{S} = -\mathbf{D} \cdot \nabla f_e + \mathbf{F} f_e. \quad (6)$$

The wave term is purely diffusive so that $\mathbf{F}_w = 0$, while the electric field term is nondiffusive: $\mathbf{D}_e = 0$,

$$\mathbf{F}_e = \frac{q_e \mathbf{E}}{m_e}. \quad (7)$$

B. Coordinate systems

Because of azimuthal symmetry, f_e is independent of ϕ the angle about the magnetic field. Two coordinate systems suggest themselves: the cylindrical coordinate system $(v_{\perp}, v_{\parallel}, \phi)$ and the spherical coordinate system (v, θ, ϕ) ; see fig. 1. These are related by

$$v^2 = v_{\perp}^2 + v_{\parallel}^2,$$

$$\cos \theta = v_{\parallel}/v.$$

Both of these coordinate systems are useful. In cylindrical coordinates (assuming azimuthal symmetry) eq. (6) gives

$$\nabla \cdot \mathbf{S} = \frac{1}{v_{\perp}} \frac{\partial}{\partial v_{\perp}} v_{\perp} S_{\perp} + \frac{\partial}{\partial v_{\parallel}} S_{\parallel}, \quad (8a)$$

$$S_{\perp} = -D_{\perp\perp} \frac{\partial f_e}{\partial v_{\perp}} - D_{\perp\parallel} \frac{\partial f_e}{\partial v_{\parallel}} + F_{\perp} f_e, \quad (8b)$$

$$S_{\parallel} = -D_{\parallel\perp} \frac{\partial f_e}{\partial v_{\perp}} - D_{\parallel\parallel} \frac{\partial f_e}{\partial v_{\parallel}} + F_{\parallel} f_e. \quad (8c)$$

Similarly, in spherical coordinates we have

$$\nabla \cdot \mathbf{S} = \frac{1}{v^2} \frac{\partial}{\partial v} v^2 S_v + \frac{1}{v \sin \theta} \frac{\partial}{\partial \theta} \sin \theta S_{\theta}, \quad (9a)$$

$$S_v = -D_{vv} \frac{\partial f_e}{\partial v} - D_{v\theta} \frac{1}{v} \frac{\partial f_e}{\partial \theta} + F_v f_e, \quad (9b)$$

$$S_{\theta} = -D_{\theta v} \frac{\partial f_e}{\partial v} - D_{\theta\theta} \frac{1}{v} \frac{\partial f_e}{\partial \theta} + F_{\theta} f_e. \quad (9c)$$

Transformations between \mathbf{D} and \mathbf{F} expressed in the two coordinate systems may be achieved by

$$\begin{pmatrix} D_{\perp\perp} \\ D_{\perp\parallel} \\ D_{\parallel\perp} \\ D_{\parallel\parallel} \end{pmatrix} = \mathbf{M} \cdot \begin{pmatrix} D_{vv} \\ D_{v\theta} \\ D_{\theta v} \\ D_{\theta\theta} \end{pmatrix} \quad (10a)$$

and

$$\begin{pmatrix} F_{\perp} \\ F_{\parallel} \end{pmatrix} = \mathbf{N} \cdot \begin{pmatrix} F_v \\ F_{\theta} \end{pmatrix}, \quad (10b)$$

where

$$\mathbf{M} = \mathbf{M}^{-1} = \begin{pmatrix} s^2 & sc & sc & c^2 \\ sc & -s^2 & c^2 & -sc \\ sc & c^2 & -s^2 & -sc \\ c^2 & -sc & -sc & s^2 \end{pmatrix}$$

$$\mathbf{N} = \mathbf{N}^{-1} = \begin{pmatrix} s & c \\ c & -s \end{pmatrix},$$

and here we have abbreviated $s = \sin \theta$ and $c = \cos \theta$. The collision term is most conveniently expressed in spherical coordinates and eqs. (10) allow us to transform this term to cylindrical coordinates. On the other hand, the rf and electric field terms are written most naturally in cylindrical coordinates, and this equation also enables us to express these terms in spherical coordinates.

In the case of the collision operator, \mathbf{D} and \mathbf{F} are given in terms of the gradients of potentials

$$\mathbf{D} \propto \nabla \nabla \psi, \quad \mathbf{F} \propto \nabla \phi.$$

In cylindrical coordinates (with azimuthal symmetry), the relevant components of \mathbf{D} and \mathbf{F} are easy to calculate—we just take the corresponding derivatives of ψ and ϕ . In spherical coordinates we have

$$(\nabla \nabla \psi)_{vv} = \frac{\partial^2 \psi}{\partial v^2}, \quad (11a)$$

$$(\nabla \nabla \psi)_{v\theta} = (\nabla \nabla \psi)_{\theta v} = \frac{1}{v} \frac{\partial^2 \psi}{\partial v \partial \theta} - \frac{1}{v^2} \frac{\partial \psi}{\partial \theta}, \quad (11b)$$

$$(\nabla\nabla\psi)_{\theta\theta} = \frac{1}{v} \frac{\partial\psi}{\partial v} + \frac{1}{v^2} \frac{\partial^2\psi}{\partial\theta^2}, \quad (11c)$$

$$(\nabla\phi)_v = \frac{\partial\phi}{\partial v}, \quad (11d)$$

$$(\nabla\phi)_\theta = \frac{1}{v} \frac{\partial\phi}{\partial\theta}. \quad (11e)$$

Several important quantities are given in terms of velocity-space moments of the distribution function. Three-dimensional velocity space integrations can be carried out in cylindrical coordinates using

$$\int f(\mathbf{v}) d^3\mathbf{v} = \int_0^\infty dv_\perp \int_{-\infty}^\infty dv_\parallel 2\pi v_\perp f(v_\perp, v_\parallel) \quad (12)$$

and in spherical coordinates using

$$\int f(\mathbf{v}) d^3\mathbf{v} = \int_0^\infty dv \int_0^\pi d\theta 2\pi v^2 f(v, \theta) \sin\theta. \quad (13)$$

C. Legendre harmonics

It is sometimes useful to decompose the distribution function and the potentials into Legendre harmonics $P_l(\cos\theta)$. We write this as

$$f(v, \theta) = \sum_{l=0}^{\infty} f^{(l)}(v) P_l(\cos\theta), \quad (14)$$

where

$$f^{(l)}(v) = \frac{2l+1}{2} \int_0^\pi f(v, \theta) P_l(\cos\theta) \sin\theta d\theta. \quad (15)$$

The Legendre polynomials may be evaluated on a computer using the recurrence relation¹⁰

$$P_0(\mu) = 1, \quad (l+1)P_{l+1}(\mu) = (2l+1)\mu P_l(\mu) - lP_{l-1}(\mu).$$

D. Definitions

Finally, we define some of the other quantities that we encounter in this paper. The thermal velocity of species s is given by

$$v_{ts} = \sqrt{\frac{T_s}{m_s}}, \quad (16)$$

where T_s is the temperature of species s . The thermal collision frequency for the electrons is

$$\nu_{te} = \tau_{te}^{-1} = \frac{\Gamma^{e/e}}{v_{te}^3}, \quad (17)$$

where

$$\Gamma^{a/b} = \frac{n_b q_a^2 q_b^2 \ln \Lambda^{a/b}}{4\pi\epsilon_0^2 m_a^2},$$

and n_s is the number density of species s , ϵ_0 is the dielectric constant of free space, and $\ln \Lambda^{a/b}$ is the Coulomb logarithm. The distributions are normalized so that

$$\int f_s(\mathbf{v}) d^3\mathbf{v} = n_s.$$

In particular, the Maxwellian distribution is

$$\begin{aligned} f_{sm}(v) &= n_s \left(\frac{m_s}{2\pi T_s} \right)^{3/2} \exp(-\frac{1}{2}m_s v^2 / T_s), \\ &= n_s \frac{1}{(2\pi v_{ts}^2)^{3/2}} \exp(-\frac{1}{2}v^2 / v_{ts}^2). \end{aligned} \quad (18)$$

In discussing the applications to rf current drive, there are two quantities in which we will be interested: the electron current density

$$J = \int q_e v_{\parallel} f_e(\mathbf{v}) d^3\mathbf{v} \quad (19)$$

and the rf power absorbed per unit volume by the plasma

$$P = \int m_e \mathbf{v} \cdot \mathbf{S}_w d^3\mathbf{v}. \quad (20)$$

The efficiency of rf current drive is usually given as the ratio J/P .

We shall use S.I. units throughout this paper except that we will measure temperature in units of energy.

III. Collision Operator

A. The Landau collision operator

The collision flux is given by the Landau collision integral¹¹

$$\mathbf{S}_c^{a/b} = \frac{q_a^2 q_b^2}{8\pi\epsilon_0^2 m_a} \ln \Lambda^{a/b} \int \mathbf{U}(\mathbf{u}) \cdot \left(\frac{f_a(\mathbf{v})}{m_b} \frac{\partial f_b(\mathbf{v}')}{\partial \mathbf{v}'} - \frac{f_b(\mathbf{v}')}{m_a} \frac{\partial f_a(\mathbf{v})}{\partial \mathbf{v}} \right) d^3\mathbf{v}', \quad (21)$$

where

$$\mathbf{U}(\mathbf{u}) = \frac{u^2 \mathbf{I} - \mathbf{u}\mathbf{u}}{u^3}, \quad \mathbf{u} = \mathbf{v} - \mathbf{v}'.$$

The formula for the Coulomb logarithm $\ln \Lambda^{a/b}$ is given in text books and the *NRL Plasma Formulary*.¹² Because it is so insensitive to plasma parameters, in many cases it is adequate to take it to be a constant equal to 15. In any case, it is required that $\ln \Lambda^{a/b} = \ln \Lambda^{b/a}$. The Landau collision operator conserves number, momentum, and energy, i.e.,

$$\int C(f_a, f_b) d^3\mathbf{v} = 0, \quad (22a)$$

$$\int m_a \mathbf{v} C(f_a, f_b) d^3\mathbf{v} + \int m_b \mathbf{v} C(f_b, f_a) d^3\mathbf{v} = 0, \quad (22b)$$

$$\int \frac{m_a v^2}{2} C(f_a, f_b) d^3\mathbf{v} + \int \frac{m_b v^2}{2} C(f_b, f_a) d^3\mathbf{v} = 0. \quad (22c)$$

There is an error on the order of $1/\ln \Lambda^{a/b}$ in the Landau collision operator. However, because it has so many “nice” properties—the conservation laws of eqs. (22), an H -theorem, etc.—it is customary to regard eq. (21) as being exact.

B. Rosenbluth potentials

Equation (21) is the most useful form for the collision operator for analytical work. However, it is not in a convenient form for numerical computations. Suppose we represent the distribution functions on an $N \times N$ grid (assuming azimuthal symmetry). Then evaluation of eq. (21) entails $O(N^4)$ computations, because it entails a two-dimensional integral (over \mathbf{v}') which must be carried out at each grid location. Fortunately, substantial savings may be realized by using an equivalent representation in terms of Rosenbluth potentials.^{13,14} Here we use the slightly more convenient notation of Trubnikov.¹⁵ We define two potentials

$$\phi_b(\mathbf{v}) = -\frac{1}{4\pi} \int \frac{f_b(\mathbf{v}')}{|\mathbf{v} - \mathbf{v}'|} d^3\mathbf{v}', \quad (23a)$$

$$\psi_b(\mathbf{v}) = -\frac{1}{8\pi} \int |\mathbf{v} - \mathbf{v}'| f_b(\mathbf{v}') d^3\mathbf{v}'. \quad (23b)$$

These are called potentials because they satisfy Poisson's equations in velocity space

$$\nabla^2 \phi_b(\mathbf{v}) = f_b(\mathbf{v}), \quad \nabla^2 \psi_b(\mathbf{v}) = \phi_b(\mathbf{v}).$$

In terms of these potentials, eq. (21) becomes

$$\mathbf{S}_c^{a/b} = -\mathbf{D}_c^{a/b} \nabla f_a(\mathbf{v}) + \mathbf{F}_c^{a/b} f_a(\mathbf{v}), \quad (24a)$$

$$\mathbf{D}_c^{a/b} = -\frac{4\pi\Gamma^{a/b}}{n_b} \nabla \nabla \psi_b(\mathbf{v}), \quad (24b)$$

$$\mathbf{F}_c^{a/b} = -\frac{4\pi\Gamma^{a/b}}{n_b} \frac{m_a}{m_b} \nabla \phi_b(\mathbf{v}). \quad (24c)$$

(An equivalent form of this equation is given by Rosenbluth *et al.*¹³ which contains a term of the form

$$\nabla \cdot [f_a(\mathbf{v}) \nabla \nabla \psi_b(\mathbf{v})].$$

This form is used in several numerical codes,²⁻⁴ even though more derivatives of ψ_b must be taken. One form may be derived from the other by noting that $\nabla^2 \psi_b = \phi_b$.)

There is an efficient method for calculating the Rosenbluth potentials. This involves decomposing f_b in Legendre harmonics eq. (15). Then we have¹³

$$\phi_b^{(l)}(v) = -\frac{1}{2l+1} \left[\int_0^v \frac{v'^{l+2}}{v'^{l+1}} f_b^{(l)}(v') dv' + \int_v^\infty \frac{v^l}{v'^{l-1}} f_b^{(l)}(v') dv' \right], \quad (25a)$$

$$\begin{aligned} \psi_b^{(l)}(v) = \frac{1}{2(4l^2-1)} & \left[\int_0^v \frac{v'^{l+2}}{v'^{l-1}} \left(1 - \frac{l-\frac{1}{2}}{l+\frac{3}{2}} \frac{v'^2}{v^2} \right) f_b^{(l)}(v') dv' \right. \\ & \left. + \int_v^\infty \frac{v^l}{v'^{l-3}} \left(1 - \frac{l-\frac{1}{2}}{l+\frac{3}{2}} \frac{v^2}{v'^2} \right) f_b^{(l)}(v') dv' \right]. \end{aligned} \quad (25b)$$

Let us assume that f_b may be represented by K Legendre harmonics (i.e., the upper limit in the sum in eq. (14) is $K-1$). Then the calculation of $f_b^{(l)}(v)$ from $f_b(\mathbf{v})$ using eq. (15) takes $O(N^2)$ computations for each l or $O(KN^2)$ computations altogether. Given $f_b^{(l)}(v)$, the calculation of $\phi_b^{(l)}(v)$ and $\psi_b^{(l)}(v)$ using eqs. (25) takes $O(N)$ computations for each l . The calculation of $\phi(\mathbf{v})$ and $\psi(\mathbf{v})$ takes a further $O(KN^2)$ step. Overall the number of steps is therefore $O(KN^2)$. Often, we can take K to be quite small (usually $K < 10$), and in any case we have $K \leq N$, so we can compute the collision term much more economically than using the Landau operator directly.

IV. Approximations to the Collision Operator

A. Isotropic background

If the background distribution is isotropic $f_b(\mathbf{v}) = f_b(v)$, then so too are ϕ and ψ . The collision term is then from eqs. (24), (25), and (11)

$$S_{cv}^{a/b} = -D_{c\theta\theta}^{a/b} \frac{\partial f_a}{\partial v} + F_{cv}^{a/b} f_a, \quad (26a)$$

$$S_{c\theta}^{a/b} = -D_{c\theta\theta}^{a/b} \frac{1}{v} \frac{\partial f_a}{\partial \theta}, \quad (26b)$$

where

$$D_{c\theta\theta}^{a/b} = \frac{4\pi\Gamma^{a/b}}{3n_b} \left(\int_0^v \frac{v'^4}{v^3} f_b(v') dv' + \int_v^\infty v' f_b(v') dv' \right), \quad (27a)$$

$$D_{c\theta\theta}^{a/b} = \frac{4\pi\Gamma^{a/b}}{3n_b} \left(\int_0^v \frac{v'^2}{2v^3} (3v^2 - v'^2) f_b(v') dv' + \int_v^\infty v' f_b(v') dv' \right), \quad (27b)$$

$$F_{cv}^{a/b} = -\frac{4\pi\Gamma^{a/b}}{3n_b} \frac{m_a}{m_b} \int_0^v \frac{3v'^2}{v^2} f_b(v') dv'. \quad (27c)$$

B. The high-velocity limit

If v is much greater than the thermal velocity of particles of species b , the indefinite limits in eqs. (27) may be replaced by infinity to give

$$D_{c\theta\theta}^{a/b} = \Gamma^{a/b} \frac{v_{tb}^2}{v^3}, \quad (28a)$$

$$D_{c\theta\theta}^{a/b} = \Gamma^{a/b} \frac{1}{2v} \left(1 - \frac{v_{tb}^2}{v^2} \right), \quad (28b)$$

$$F_{cv}^{a/b} = -\Gamma^{a/b} \frac{m_a}{m_b} \frac{1}{v^2}, \quad (28c)$$

where the thermal velocity is defined for an arbitrary isotropic distribution as

$$v_{ts}^2 = \frac{4\pi}{3n_s} \int_0^\infty v^4 f_s(v) dv. \quad (29)$$

[For a Maxwellian distribution, eq. (18), this reduces to the usual expression eq. (16).]

C. Maxwellian background

If the background distribution is Maxwellian eq. (18), the integrals in eq. (27) can be carried out to give¹⁵

$$D_{c\theta\theta}^{a/b} = \frac{\nu_{\parallel}^{a/b}}{2} v^2 = \frac{\Gamma^{a/b}}{2v} \left(\frac{\text{erf}(u)}{u^2} - \frac{\text{erf}'(u)}{u} \right), \quad (30a)$$

$$D_{c\theta\theta}^{a/b} = \frac{\nu_{\perp}^{a/b}}{4} v^2 = \frac{\Gamma^{a/b}}{4v} \left(\left(2 - \frac{1}{u^2} \right) \text{erf}(u) + \frac{\text{erf}'(u)}{u} \right), \quad (30b)$$

$$F_{cv}^{a/b} = -\frac{m_a}{m_a + m_b} \nu_s^{a/b} v = -\frac{\Gamma^{a/b}}{v^2} \frac{m_a}{m_b} [\text{erf}(u) - u \text{erf}'(u)], \quad (30c)$$

where

$$\begin{aligned}\operatorname{erf}(u) &= \frac{2}{\sqrt{\pi}} \int_0^u \exp(-x^2) dx, \\ \operatorname{erf}'(u) &= \frac{2}{\sqrt{\pi}} \exp(-u^2), \\ u &= \frac{v}{\sqrt{2}v_{tb}}.\end{aligned}$$

The parallel diffusion rate $\nu_{\parallel}^{a/b}$, perpendicular diffusion rate $\nu_{\perp}^{a/b}$, and the slowing down diffusion rate $\nu_s^{a/b}$ are the same as those defined in the *NRL Plasma Formulary*.¹² [However, the *NRL Plasma Formulary* (1983 edition) has an incorrect formula for the collision operator with a Maxwellian background.]

For $u > 0$, $\operatorname{erf}(u)$ is given approximately by¹⁰

$$\operatorname{erf}(u) = 1 - \exp(-u^2) \sum_{k=1}^5 a_k t^k,$$

where

$$t = 1/(1 + pu)$$

and

$$\begin{aligned}p &= 0.32759\ 11, \\ a_1 &= 0.25482\ 9592, & a_2 &= -0.28449\ 6736, \\ a_3 &= 1.42141\ 3741, & a_4 &= -1.45315\ 2027, \\ a_5 &= 1.06140\ 5429.\end{aligned}$$

This approximation cannot be used in evaluating eqs. (30) near $u = 0$ because there is cancellation to leading order in all three terms. In that case, the Taylor expansion,

$$\begin{aligned}\operatorname{erf}(u) - u \operatorname{erf}'(u) &= \frac{2}{\sqrt{\pi}} \sum_{k=0}^{\infty} \frac{(-1)^k}{k!} \frac{2}{2k+3} u^{2k+3} \\ &= \frac{2}{\sqrt{\pi}} \left(\frac{2}{3} u^3 - \frac{2}{5} u^5 + \frac{1}{7} u^7 - \frac{1}{27} u^9 + \dots \right),\end{aligned}$$

may be used. Alternatively, we can compute eqs. (30) by numerically evaluating the integrals in eqs. (27) with $f_b(v) = f_{bm}(v)$. This method is then easily extended to include relativistic effects as given in sec. X.

The ratio $F_{cv}^{a/b}/D_{cv}^{a/b}$ from eqs. (30) [and also (28)] is $-m_a v/T_b$ so that the effect of collisions with species b is to make species a approach a Maxwellian with temperature T_b .

D. Linearized collision operator

In many applications in plasma physics (including those involving rf waves) collisions dominate the thermal particles. Therefore, the distribution function may be expanded about a Maxwellian

$$f_a(\mathbf{v}) = f_{am}(v) + f_{a1}(\mathbf{v}).$$

The self-collision operator $C(f_a, f_a)$ may be approximated by the linearized operator

$$C_{\text{lin}}^{a/a}(f_a(\mathbf{v})) = C(f_a(\mathbf{v}), f_{am}(v)) + C(f_{am}(v), f_a(\mathbf{v})), \quad (31)$$

where we have made use of the fact that $C(f_{am}, f_{am}) = 0$, and we have ignored terms of order f_{a1}^2 . We can compute $C(f_a(\mathbf{v}), f_{am}(v))$ using eqs. (26) and (30). To compute $C(f_{am}(v), f_a(\mathbf{v}))$, we express $f_a(\mathbf{v})$ as a sum of Legendre harmonics, eq. (14), to give

$$C(f_{am}(v), f_a(\mathbf{v})) = \sum_{l=0}^{\infty} C(f_{am}(v), f_a^{(l)}(\mathbf{v}) P_l(\cos \theta)). \quad (32)$$

The zeroth term in the sum can be computed using eqs. (26) and (27) giving

$$\begin{aligned} \frac{C(f_{am}(v), f_a^{(0)}(v))}{f_{am}(v)} &= \frac{4\pi\Gamma^{a/a}}{n_a} \left[f_a^{(0)}(v) + \int_0^v \frac{v'^2}{v_{ta}^2} f_a^{(0)}(v') \left(\frac{v'^2}{3v_{ta}^2 v} - \frac{1}{v} \right) dv' \right. \\ &\quad \left. + \int_v^{\infty} \frac{v'^2}{v_{ta}^2} f_a^{(0)}(v') \left(\frac{v^2}{3v_{ta}^2 v'} - \frac{1}{v'} \right) dv' \right]. \end{aligned} \quad (33)$$

The next term in the sum in eq. (32) is given by eqs. (24), (25), and (11)

$$\begin{aligned} \frac{C(f_{am}(v), f_a^{(1)}(v) \cos \theta)}{f_{am}(v) \cos \theta} &= \frac{4\pi\Gamma^{a/a}}{n_a} \left[f_a^{(1)}(v) + \int_0^v \frac{v'^2}{v_{ta}^2} f_a^{(1)}(v') \left(\frac{v'^3}{5v_{ta}^2 v^2} - \frac{v'}{3v^2} \right) dv' \right. \\ &\quad \left. + \int_v^{\infty} \frac{v'^2}{v_{ta}^2} f_a^{(1)}(v') \left(\frac{v^3}{5v_{ta}^2 v'^2} - \frac{v}{3v'^2} \right) dv' \right]. \end{aligned} \quad (34)$$

The corresponding fluxes for this term are

$$\begin{aligned} \frac{S_v^{a/a}}{f_{am}(v) \cos \theta} &= \frac{4\pi\Gamma^{a/a}}{n_a} \left[\int_0^v f_a^{(1)}(v') \left(\frac{v'^5}{5v_{ta}^2 v^3} - \frac{2v'^3}{3v^3} \right) dv' \right. \\ &\quad \left. + \int_v^{\infty} f_a^{(1)}(v') \left(\frac{v^2}{5v_{ta}^2} + \frac{1}{3} \right) dv' \right], \end{aligned} \quad (35a)$$

$$\begin{aligned} \frac{S_{\theta}^{a/a}}{f_{am}(v) \sin \theta} &= \frac{4\pi\Gamma^{a/a}}{n_a} \left[\int_0^v f_a^{(1)}(v') \left(\frac{v'^5}{10v_{ta}^2 v^3} - \frac{v'^3}{6v_{ta}^2 v} - \frac{v'^3}{3v^3} \right) dv' \right. \\ &\quad \left. - \int_v^{\infty} f_a^{(1)}(v') \left(\frac{v^2}{15v_{ta}^2} + \frac{1}{3} \right) dv' \right]. \end{aligned} \quad (35b)$$

Because of conservation of number, momentum, and energy, the solutions to the homogeneous equation

$$C_{\text{lin}}^{a/a}(f_a(\mathbf{v})) = 0$$

are

$$f_a(\mathbf{v}) = (a + \mathbf{b} \cdot m_a \mathbf{v} + d \frac{1}{2} m_a v^2) f_{am}(v).$$

If we substitute $a = \mathbf{b} = 0$, we obtain a check on eq. (33). Similarly, $a = d = 0$ and $\mathbf{b} = \hat{\mathbf{v}}_{\parallel}$ gives a check on eq. (34). Such checks are useful when incorporating the linearized collision operator into a numerical code.

E. Electron-ion collision operator

We now turn to the specific problem of current drive by lower hybrid waves. In this problem we wish to solve the Fokker–Planck equation for the electrons including the effects of electron-ion and electron-electron collisions.

Because the ions are so massive relative to the electrons, we have $v \gg v_{ti}$ for nearly all the electrons and eqs. (28) apply. Indeed, we can make the further approximations $m_i \rightarrow \infty$, $v_{ti} \rightarrow 0$, in which case the collision operator is given by eq. (26) with

$$D_{cvv}^{e/i} = F_{cv}^{e/i} = 0, \quad (36a)$$

$$D_{c\theta\theta}^{e/i} = \Gamma^{e/e} \frac{Z_i}{2v}, \quad (36b)$$

where

$$Z_i = -\frac{q_i \ln \Lambda^{e/i}}{q_e \ln \Lambda^{e/e}},$$

and we have assumed neutrality $q_e n_e + q_i n_i = 0$. The full electron-ion collision term $C(f_e, f_i)$ can be written as

$$C^{e/i}(f_e(\mathbf{v})) = \Gamma^{e/e} \frac{Z_i}{2v^3} \frac{1}{\sin \theta} \frac{\partial}{\partial \theta} \sin \theta \frac{\partial}{\partial \theta} f_e(\mathbf{v}). \quad (37)$$

For a multispecies plasma Z_i is replaced by Z_{eff} where

$$Z_{\text{eff}} = \frac{\sum_s n_s q_s^2 \ln \Lambda^{e/s}}{n_e q_e^2 \ln \Lambda^{e/e}},$$

and the sum extends over all the ionic species.

With this collision operator the ions are characterized by a single dimensionless parameter Z_i (or Z_{eff}). The collision operator allows momentum to be transferred from the electrons to the ions, but there is no energy exchange. The non-negative nature of f_e is preserved.

F. Electron-electron collision operator

There are several choices for the electron-electron collision operator. We will discuss them starting at the most complex.

The *full* electron-electron collision operator is given by eqs. (24) and (25). This was first used in current-drive studies by Harvey *et al.*¹⁶ This collision operator conserves both momentum and energy. The electron distribution f_e remains non-negative. Because the collision operator conserves energy, there is nowhere for rf energy absorbed by the electrons to go. The problem arises because we have reduced a problem in configuration and velocity space to one in velocity space alone, so that there is now no spatial diffusion of energy. In practice, this problem is solved by inserting an energy loss term into the Fokker–Planck eq. (1). Unfortunately, there are several different models for this loss term and so this procedure is somewhat *ad hoc*.

The *linearized* electron-electron collision operator is given by eq. (31). This too conserves momentum and energy. The non-negative nature of f_e is no longer preserved. When the perturbation to f_{em} is small, f_e usually only becomes negative far out on the tail. The energy conservation of the collision operator again necessitates the introduction of an energy loss term. Fortunately, there is a systematic way to do this within the context of a Chapman–Enskog–Braginskii expansion.^{17,18} The energy loss term has the form

$$-\left(\frac{m_e v^2}{2T_e} - \frac{3}{2}\right) f_{em}(v) \frac{\partial \ln T_e}{\partial t},$$

which appears on the right-hand side of eq. (1). Operationally, $\partial \ln T_e / \partial t$ would be adjusted to ensure that the energy of the electron distribution $f_e(\mathbf{v})$ remained constant. (In fact, one of the results of the expansion procedure is an equation for the evolution of T_e including the effects of rf and ohmic heating and of energy transport.)

A useful modification of this collision operator is the *truncated* collision operator

$$C_{\text{trunc}}^{e/e}(f_e(\mathbf{v})) = C(f_e(\mathbf{v}), f_{em}(v)) + C(f_{em}(v), f_e^{(1)}(v) \cos \theta), \quad (38)$$

where the first term is given by eqs. (26) and (30) and the second term by eq. (34). This differs from the linearized operator in that we only retain the $l = 0$ and $l = 1$ terms in the sum in eq. (32) and we further approximate $f_e^{(0)}(v)$ by $f_{em}(v)$. As a consequence, this operator conserves momentum but not energy; so there is no need to introduce an energy loss term. Again, the electron distribution function may become negative. This collision operator is useful in the study of current drive by low-phase-velocity waves and in the treatment of problems with an electric field. In both of these examples, a momentum-conserving electron-electron collision operator is required. This operator was used (in a relativistic form) in the study of current drive by fast waves.¹⁹

A slightly different technique for ensuring momentum conservation was used in our study of current drive by low-phase-velocity waves.²⁰ There we approximated the electron-electron collision operator by

$$C_{\text{drift}}^{e/e}(f_e(\mathbf{v})) = C(f_e(\mathbf{v}), f_{em}(|\mathbf{v} - v_d \hat{\mathbf{v}}_{\parallel}|)),$$

where the background is a *drifting* Maxwellian with a drift speed v_d adjusted so that the parallel force between $f_e(\mathbf{v})$ and the drifting Maxwellian,

$$P_{\parallel}^{e/e} = \int m_e S_{\parallel}^{e/e} d^3 \mathbf{v}, \quad (39)$$

vanishes. This collision operator conserves momentum (by construction) and preserves the non-negative nature of f_e . Energy is not conserved. It is, however, slightly less accurate than the truncated operator. In particular, while the truncated operator gives the correct value for the electrical conductivity,²¹ this operator gives an answer which is in error by about 15%. The computation of this collision operator involves computing eqs. (30) in the drifting frame, converting to cylindrical coordinates using eqs. (10), transforming to the rest frame (which is easy in cylindrical coordinates), and finally converting back to spherical coordinates using eqs. (10). In order to determine the drift speed, we use the analytical formula for the force on an electron Maxwellian drifting with speed v_d due to a stationary ion background, i.e.,

$$P_{\parallel}^{e/i} = -n_e m_e \nu_{te} v_d Z_i \frac{1}{3} \sqrt{\frac{2}{\pi}} \sqrt{\frac{m_i}{m_i + m_e}},$$

which is valid for $|v_d| \ll v_{te}$. Here we have taken the mass ratio m_e/m_i to be finite and have assumed that $T_i = T_e$. The force between two electron Maxwellians with a relative drift of v_d is found by taking $Z_i = 1$ and $m_i = m_e$ which gives

$$P_{\parallel}^{e/e} = -\frac{n_e m_e \nu_{te} v_d}{3\sqrt{\pi}}. \quad (40)$$

In the numerical code $P_{\parallel}^{e/e}$ is computed using eq. (39). Equation (40) is used to estimate the *change* in v_d required to give $P_{\parallel}^{e/e} = 0$.

The situation may be further simplified by assuming that the background electrons are *Maxwellian*, so that the collision operator is given by

$$C_{\text{Max}}^{e/e}(f_e(\mathbf{v})) = C(f_e(\mathbf{v}), f_{em}(v)), \quad (41)$$

which may be evaluated using eqs. (26) and (30). This operator conserves neither energy nor momentum. It does preserve the non-negative nature of f_e . It was used by Kulsrud *et al.*⁵ in the study of runaways, and in studies of lower hybrid current drive.⁶ The Maxwellian background serves as a heat bath, so

no energy loss terms are required. The absence of momentum conservation introduces approximately a factor-of-two error in the electrical conductivity⁵ and in the efficiency of current drive by slow waves.²⁰ There is a relative error of order $(v_{te}/v)^3$ in the determination of the current-drive efficiency for fast waves.¹⁹

Lastly, $C_{\text{Max}}^{e/e}$ may be approximated by using the *high* velocity limit, i.e., by using eqs. (28) instead of eqs. (30). In fact, because eq. (28b) gives negative diffusion for small v , it is usually replaced by

$$D_{c\theta\theta}^{a/b} = \Gamma^{a/b} \frac{1}{2v}.$$

We define the resulting electron-electron collision operator as $C_{\text{high}}^{e/e}$. It has much the same properties as $C_{\text{Max}}^{e/e}$. In particular, it yields a Maxwellian (with temperature T_e) as the steady-state solution. Because of the greater error in the collision term for thermal particles the electrical conductivity is even lower than for $C_{\text{Max}}^{e/e}$. The evaluation of eqs. (28) is, of course, a little easier to program than that of eqs. (30). However, because the results of evaluating eqs. (30) can be stored in a table, the extra computational cost of working with $C_{\text{Max}}^{e/e}$ is insignificant compared to the solution of the Fokker–Planck equation. Since $C_{\text{high}}^{e/e}$ is less accurate, its use is not recommended for numerical work. It is, however, useful in analytical work.

When working with these electron-electron collision operators, it is useful to have some benchmark against which to check their numerical realization. A useful benchmark is provided by the electrical conductivity, which is the ratio of electrical current to electric field in the limit $E \rightarrow 0$. This is tabulated in table I for various values of Z_i and for all the electron-electron collision operators discussed here. These values were obtained by solving the corresponding one-dimensional equation by the method outlined in sec. XI. In all cases, the electron-ion collision operator is given by eq. (37). The conductivity using the full and the truncated electron-electron collision operators is the same as for the linearized operator. In the limit $Z_i \rightarrow \infty$, the conductivity is independent of the electron-electron collision model

$$\frac{J}{E} = 16 \sqrt{\frac{2}{\pi}} \frac{1}{Z_i} \frac{n_e q_e^2}{m_e \nu_{te}}.$$

For the high-velocity approximation to the collision operator the conductivity can be expressed analytically as

$$\frac{J}{E} = \frac{16}{3} \sqrt{\frac{2}{\pi}} \frac{3Z_i + 13}{(Z_i + 3)(Z_i + 5)} \frac{n_e q_e^2}{m_e \nu_{te}}.$$

V. Quasilinear Operator

A. Single wave

The interaction of electrons (or other species) with a wave is conveniently described in terms of the quasilinear theory.²² In this theory the flux of electrons in velocity space is given by

$$\mathbf{S}_w = -\mathbf{D}_w \cdot \nabla f_e, \quad (42)$$

where \mathbf{D}_w is the quasilinear diffusion tensor which depends on the waves present in the plasma. Although quasilinear theory is not strictly applicable to a single wave, we will start with this case because it is the simplest. Suppose there is a uniform wave present in the plasma, i.e.,

$$\mathbf{E}(\mathbf{r}, t) = \text{Re}[\mathbf{E}_w \exp(i\mathbf{k} \cdot \mathbf{r} - i\omega t)]. \quad (43)$$

The quasilinear diffusion coefficient is given by²²

$$\mathbf{D}_w = \sum_n \frac{\pi}{2} \frac{q_e^2}{m_e^2} \delta(\omega - k_{\parallel} v_{\parallel} - n\Omega_e) \mathbf{a}_n^* \mathbf{a}_n \quad (44)$$

and

$$\begin{aligned} \mathbf{a}_n &= \Theta_n \frac{k_{\parallel}}{\omega} \left[\left(\frac{\omega}{k_{\parallel}} - v_{\parallel} \right) \hat{\mathbf{v}}_{\perp} + v_{\perp} \hat{\mathbf{v}}_{\parallel} \right] \\ \Theta_n &= \frac{E_{w+} J_{n-1} + E_{w-} J_{n+1}}{\sqrt{2}} + \frac{v_{\parallel}}{v_{\perp}} J_n E_{w\parallel}, \end{aligned}$$

where $\Omega_e = q_e B / m_e$ is the electron cyclotron frequency, B is the magnetic field, $*$ indicates complex conjugation, J_n is the n th order Bessel function, and the argument of the Bessel functions is $k_{\perp} v_{\perp} / \Omega_e$. E_{w+} and E_{w-} are the left- and right-handed components of \mathbf{E}_w ; in a right-handed cartesian coordinate system with $\hat{\mathbf{z}}$ parallel to \mathbf{B} and \mathbf{k} lying in the (x, z) plane, we have

$$\begin{aligned} E_{w+} &= \frac{E_{wx} + iE_{wy}}{\sqrt{2}}, \\ E_{w-} &= \frac{E_{wx} - iE_{wy}}{\sqrt{2}}, \\ E_{w\parallel} &= E_{wz}. \end{aligned}$$

It is instructive to consider the properties of eq. (44). The delta function specifies the resonance condition. Only particles for which the Doppler-shifted wave frequency $\omega - k_{\parallel} v_{\parallel}$ is zero ($n = 0$ —the Landau resonance) or a multiple of the cyclotron frequency ($n \neq 0$ —a cyclotron harmonic resonance) interact with the wave. The vector \mathbf{a}_n is perpendicular to the velocity of the electron in the wave frame $\mathbf{v} - (\omega/k_{\parallel}) \hat{\mathbf{v}}_{\parallel}$. This means that the wave-induced flux is along diffusion paths which lie in constant-energy surfaces in the wave frame; see fig. 2. Similarly, the flux is proportional to the gradient in f_e in this direction. As a consequence, when an electron interacts with a particle via the Landau resonance, the diffusion tensor consists of only a single component

$$\mathbf{D}_w = D_{\parallel\parallel} \hat{\mathbf{v}}_{\parallel} \hat{\mathbf{v}}_{\parallel}.$$

Likewise, for a cyclotron harmonic resonance, we have

$$\mathbf{D}_w = D_{\perp\perp} \hat{\mathbf{v}}_{\perp} \hat{\mathbf{v}}_{\perp},$$

provided that v_{\perp} is small compared with $n\Omega_e/k_{\parallel}$.

The appearance of the delta function in eq. (44) is a consequence of the assumed uniformity of the magnetic field. In this case, v_{\parallel} is a constant of the unperturbed motion and so a particle remains in resonance for a long time. In situations described by bounce-averaged codes, the magnetic field and v_{\parallel} vary along a particle orbit so that the particle does not remain in resonance. This effect can be taken into account by averaging eq. (44) along a particle trajectory.²³ This removes the delta function, although there are still singularities in the resulting expression arising from those particles which turn in the resonance.⁸

B. Many waves

Equation (44) is easily generalized to include a more realistic representation of the wave fields. An important application is to the incorporation of quasilinear effects into a ray-tracing code. Here the externally injected rf power is represented by several rays. Let us consider the interaction of these waves

with the electrons on a particular flux surface. At the point where a given ray intersects the flux surface it is characterized by its position \mathbf{r} , wave number \mathbf{k} , and power W (usually the frequency ω is fixed by the rf source). W measures the number of watts carried by the ray. In order to apply eq. (44), we must determine the amplitude of the corresponding single wave \mathbf{E}_w which has the same polarization and same rms field amplitude as the ray (with the rms averaging performed over time and over the flux surface).

The ray contributes

$$U = \frac{W}{|\mathbf{v}_g \cdot \hat{\mathbf{n}}| A_f}$$

to the wave energy density (in J/m³) averaged over the flux surface, where \mathbf{v}_g is the group velocity of the ray, $\hat{\mathbf{n}}$ is the unit vector normal to surface at the point of intersection and A_f is the area of the flux surface. The polarization of the electric field is given by

$$\mathbf{K} \cdot \mathbf{E}_w = 0,$$

where

$$\mathbf{K} = \frac{c^2}{\omega^2}(\mathbf{k}\mathbf{k} - k^2\mathbf{I}) + \mathbf{I} + i \frac{\boldsymbol{\sigma}(\mathbf{k}, \omega)}{\omega\epsilon_0}$$

is the dispersion tensor, c is the velocity of light, and $\boldsymbol{\sigma}(\mathbf{k}, \omega)$ is the conductivity tensor. The energy density is related to \mathbf{E}_w by²⁴

$$U = \frac{1}{4}\epsilon_0\omega\mathbf{E}_w^* \cdot \frac{\partial\mathbf{K}}{\partial\omega} \cdot \mathbf{E}_w.$$

Given W , we can therefore determine \mathbf{E}_w (to within an ignorable phase factor) appropriately averaged over the flux surface.

This is substituted into eq. (44) and the result summed over all the rays to give the overall quasi-linear diffusion tensor. In practice, the delta-functions appearing in this expression must be replaced by smoothed functions. This allows the ray-tracing procedure to reflect the true situation in which a continuous spectrum of waves is launched.

We complete the discussion of the ray-tracing by pointing out that the damping of the rays should be calculated self-consistently from \mathbf{D}_w . The power that a particular ray loses per unit volume due to absorption by the electrons is given by eq. (20), where instead of the total \mathbf{S}_w we use the contribution the ray in question makes to \mathbf{S}_w . To this should be added the power absorbed by the other species if applicable. Then the ray power W satisfies the equation

$$\frac{dW}{dt} = -P |\mathbf{v}_g \cdot \hat{\mathbf{n}}| A_f,$$

where the time derivative is the derivative taken along the ray.

If instead of a discrete set of waves, the wave fields are given by a spectrum

$$\mathbf{E}(\mathbf{r}, t) = \int \mathbf{E}_w(\mathbf{k}) \exp[i\mathbf{k} \cdot \mathbf{r} - i\omega(\mathbf{k})t] \frac{d^3\mathbf{k}}{(2\pi)^3},$$

then eq. (44) becomes²²

$$\mathbf{D}_w = \sum_n \frac{q_e^2}{m_e^2} \int \frac{d^3\mathbf{k}}{(2\pi)^3} \frac{1}{V_p} \pi \delta[\omega(\mathbf{k}) - k_{\parallel} v_{\parallel} - n\Omega_e] \mathbf{a}_n^* \mathbf{a}_n, \quad (45)$$

where V_p is the configuration space volume of the plasma and the definition of \mathbf{a}_n is generalized in the obvious way.

C. Model forms

The results given above allow a ray-tracing code to be coupled to the solution of the Fokker–Planck equation. This is an extremely complicated system, and much work has been carried out using assumed forms for the quasilinear diffusion coefficient. This allows us to study the physics of the interaction of the electrons and the waves without having to worry about the additional physics of the wave propagation. The most widely used model form for lower hybrid waves was introduced by Fisch¹ and is given by

$$\mathbf{D}_w = D_w(v_{\parallel}) \hat{\mathbf{v}}_{\parallel} \hat{\mathbf{v}}_{\parallel}, \quad (46a)$$

where

$$D_w(v_{\parallel}) = \begin{cases} D_0, & \text{for } v_1 < v_{\parallel} < v_2, \\ 0, & \text{otherwise.} \end{cases} \quad (46b)$$

This form of \mathbf{D}_w is justified as follows. Because lower hybrid waves interact only via the Landau resonance, only the $\hat{\mathbf{v}}_{\parallel} \hat{\mathbf{v}}_{\parallel}$ component is present. If $k_{\perp} v_{te} / \Omega_e \ll 1$, the dependence on perpendicular velocity may be ignored ($J_0 \approx 1$). Finally, in many cases, the magnitude of the quasilinear diffusion greatly dominates over the collisions; thus the quasilinear diffusion coefficient tends to make an abrupt transition (in velocity space) from being negligible to being large; if D_0 is sufficiently large (i.e., large enough to form a quasilinear plateau), this situation is accurately modeled by eq. (46b).

This particular form for \mathbf{D}_w is useful because much theoretical work has been carried out using it.¹ Numerical solutions to the Fokker–Planck equation provide the best test of these theories. It is therefore important that any numerical code be able to handle the discontinuities in \mathbf{D}_w . (Note, however, that both f_e and \mathbf{S} are continuous even if \mathbf{D}_w is not.)

This model is readily generalized, for example, by allowing $D_0(v_{\parallel})$ to be an arbitrary function. Thus the effect of a backward component to the lower hybrid spectrum can be studied by including another boxlike component to D_0 . Similar models have been used to study low-phase-velocity current drive²⁰ and electron-cyclotron current drive.²⁵

D. Direct specification of the quasilinear flux

Both analytical and numerical studies show that the current drive efficiency is primarily determined by the location at which electrons interact with the waves and the direction in which the waves push the electrons. It is sometimes useful to specify the rf-induced flux directly as some arbitrary vector field $\mathbf{S}_w(\mathbf{v})$. Indeed, in some cases we may know \mathbf{S}_w more accurately than we know \mathbf{D}_w . In a ray-tracing calculation, \mathbf{D}_w may be calculated self-consistently in terms of the power flows in the various rays. However, in cruder zero-dimensional calculations, we may wish to assert merely that so much rf power is absorbed by the electrons. Then \mathbf{S}_w may be estimated from eq. (20) using an *a priori* knowledge of which electrons interact with the waves. Alternatively, \mathbf{S}_w may be estimated from either an approximate analytic solution of the Fokker–Planck equation²⁶ or from a solution of the one-dimensional Fokker–Planck equation.¹

If \mathbf{S}_w is given, then the Fokker–Planck equation (1) is an inhomogeneous (instead of homogeneous) equation. However, assuming that one of the linear electron–electron collision operators is being used, the linear operator acting on f_e in eq. (1) is now independent of the wave drive. This property is used in the adjoint methods to provide a very efficient method of solving for moments of f_e (see sec. XI).

VI. Boundary Conditions

A. Computational domain

We shall take the computational domain V for the Fokker–Planck equation to be

$$0 < v_{\perp} < v_{\perp\max}, \quad v_{\parallel\min} < v_{\parallel} < v_{\parallel\max}, \quad (47)$$

for problems solved in a cylindrical coordinate system and

$$0 < v < v_{\max}, \quad 0 < \theta < \pi, \quad (48)$$

for problems solved in a spherical coordinate system. The boundary of V is defined to be A . (For example, in spherical coordinates, A is the spherical surface $v = v_{\max}$.)

B. Internal boundaries

We distinguish two types of boundary: internal and external boundaries. The internal boundaries are the simplest. In a cylindrical coordinate system we have an internal boundary at $v_{\perp} = 0$. Values of f beyond this boundary are determined by symmetry

$$f_e(-v_{\perp}, v_{\parallel}) = f_e(v_{\perp}, v_{\parallel}). \quad (49)$$

Similarly, in spherical coordinates we have internal boundaries at $v = 0$ and at $\theta = 0$ and $\theta = \pi$. These boundaries are treated with the boundary conditions

$$f_e(-v, \theta) = f_e(v, \pi - \theta), \quad (50a)$$

$$f_e(v, -\theta) = f_e(v, \theta), \quad (50b)$$

$$f_e(v, \pi + \theta) = f_e(v, \pi - \theta). \quad (50c)$$

C. External boundaries

The other boundaries are inserted into the problem in violation of the true physical picture. In reality the velocity domain extends off to infinity; on the computer, however, we normally study only a subspace. We have to choose the subspace to include all the interesting physics: for studies of electron distribution in a spherical coordinate system, we require $v_{\max} \gg v_{te}$; if the electrons are driven by lower hybrid waves, then we further require $v_{\max} > (\omega/k_{\parallel})_{\max}$, the maximum wave phase velocity; if we wish to study runaways, then v_{\max} must exceed the runaway velocity; and so on. We next have to choose boundary conditions which are as “innocuous” as possible; i.e., which perturb the solution in the domain of integration as little as possible compared to the solution in the full domain.

For electron current-drive problems we choose the condition

$$\mathbf{S} \cdot \hat{\mathbf{n}} = 0, \quad (51)$$

on the external boundary A , where $\hat{\mathbf{n}}$ is the normal to A . This means that plasma cannot enter or leave the domain of integration. Thus the number of electrons is conserved with this boundary condition. This boundary condition gives a Maxwellian steady state in the absence of the rf, and allows a steady-state solution to be reached in the presence of rf.

If an electric field is present, then in the real problem some electrons will run away. Now we wish to impose boundary conditions which “allow” this to happen. At the boundary we have $v \gg v_{te}$ so that collisions are weak, and the dominant process is the acceleration by the electric field (we assume that the

boundary is removed from the region where the rf diffusion takes place). The Fokker–Planck equation then reduces to a hyperbolic equation. The tactic is to apply the same boundary condition as before, namely eq. (51), where the characteristics of the hyperbolic system enter the domain of integration. Where the characteristics leave, we set those diffusion terms which lead to a flux across the boundary to zero. This makes the equation purely hyperbolic in the direction normal to the boundary and so *no* boundary condition is required. (We shall see in sec. VII how this comes about in the numerical scheme.)

If we assume that $q_e E > 0$ so that electrons run away in the positive direction, then in cylindrical coordinates we would impose

$$\begin{aligned} S_{\parallel} &= 0, & \text{for } v_{\parallel} &= v_{\parallel\text{min}}, \\ S_{\perp} &= 0, & \text{for } v_{\perp} &= v_{\perp\text{max}}, \\ D_{\parallel\perp} = D_{\parallel\parallel} &= 0, & \text{for } v_{\parallel} &= v_{\parallel\text{max}}. \end{aligned} \quad (52)$$

(The boundary at $v_{\perp} = v_{\perp\text{max}}$ is taken to be an incoming boundary because the small collisional friction makes the characteristics enter along this boundary.)

A slightly more accurate treatment is possible in spherical coordinates. If we compare the various collision terms in the high-velocity limit eqs. (28), we find $F_{cv} \sim D_{c\theta\theta}/v \sim 1/v^2$ and $D_{c\theta\theta}/v \sim v_{te}^2/v^4$. Thus we can ignore the energy diffusion term $D_{c\theta\theta}$ compared with the other collisional terms. The pitch-angle scattering term $D_{c\theta\theta}$ requires no special handling because it causes diffusion parallel to the boundary. The equation is, therefore, hyperbolic in the direction perpendicular to the boundary with a characteristic acceleration given by $F_v = F_{cv} + (q_e E/m_e) \cos \theta$. The boundary conditions on $v = v_{\text{max}}$ then become

$$\begin{aligned} S_v &= 0, & \text{for } F_v &< 0, \\ D_{vv} = D_{v\theta} &= 0, & \text{for } F_v &> 0. \end{aligned} \quad (53)$$

For $v_{\text{max}} \gg v_{te}$, F_{cv} is accurately approximated by eq. (28c) (with $a = b = e$). Thus, if $|E| < m_e \Gamma^{e/e} / |q_e| v_{\text{max}}^2$, this boundary condition reduces to eq. (51), allowing problems involving both an electric field and rf diffusion to be handled in a unified way. In this small electric field limit, $S_v = 0$ is zero everywhere on the boundary and the numerical runaway rate vanishes. This is a close approximation to the true situation in which the runaway rate is exponentially small—on the order of $\exp(-v_{\text{max}}^2/v_{te}^2)$.

D. Treatment of runaways

With a finite boundary, we can determine the runaway rate accurately (provided v_{max} is sufficiently large). However, the behavior of the runaways beyond the boundary is not followed. One could, of course, just choose a very large boundary; but this is wasteful of computer resources and really just postpones the time at which the problem is encountered. It is, therefore, preferable to treat the runaways as a separate species. Assuming that the runaways are affected only by the electric field, the density and current moments of the runaway population form a closed set of equations. We define

$$\begin{aligned} n_r &= \int_{\bar{V}} f_e d^3\mathbf{v}, \\ J_r &= \int_{\bar{V}} q_e v_{\parallel} f_e d^3\mathbf{v}, \end{aligned}$$

where \bar{V} is the complement of V , i.e., the region $v > v_{\text{max}}$ in spherical coordinates. Applying eqs. (5a) and (5b) to \bar{V} we find

$$\begin{aligned} \frac{\partial n_r}{\partial t} &= \int_A \mathbf{S} \cdot d^2\mathbf{A}, \\ \frac{\partial J_r}{\partial t} &= \frac{q_e^2 E}{m_e} n_r + \int_A q_e v_{\parallel} \mathbf{S} \cdot d^2\mathbf{A}. \end{aligned}$$

Thus if we wish to determine the total current as a function of time, we need only supplement the Fokker–Planck equation by two ordinary differential equations and then sum the nonrunaway and runaway contributions to the current.

VII. Spatial Differencing

A. Choice of coordinate system

We have discussed both the cylindrical and the spherical coordinate systems. Which one should be used in a given application? The numerical scheme that is described here works best if the diffusion tensor is nearly diagonal. Then the mixed derivative terms in eqs. (8) or (9) are small. (It is these terms which tend to make the numerical scheme unstable.) Now the collision operator is approximately diagonal in spherical coordinates while the quasilinear term is nearly diagonal in cylindrical coordinates. Thus the choice of coordinate system to some extent depends on the relative strength of these two terms. Cylindrical coordinates were used in the study of current drive by low-phase-velocity waves²⁰ because the edges of the resonant region line up with coordinate lines allowing the scaling with phase velocity to be measured more accurately. On the whole, however, the spherical system is to be preferred because the electron-ion collision term eq. (37) becomes large near $v = 0$ and we wish this term to be diagonal. In ref. 20 much smaller time steps had to be taken to avoid the problem with the electron-ion term. The boundary conditions can also be applied more accurately in spherical coordinates when an electric field is present [eqs. (53)]. For this reason, we will focus on the spherical coordinate system in this section. Extension to the cylindrical coordinate system is straightforward.

An alternate representation of f_e is as a series of Legendre harmonics. This has no particular merit in quasilinear problems because the sharp gradients in \mathbf{D}_w , eq. (46), cause the Legendre expansion to be slowly convergent.

B. Normalizations

In solving equations of physical significance on the computer, it is often useful to normalize all the physical quantities. This allows us to work with numbers which are closer to unity (and thus avoid potential problems due to arithmetic overflow or underflow); more importantly, the number of parameters needed to specify the problem is often reduced.

For the problem of current drive by lower hybrid waves, we solve the Fokker–Planck equation for the electrons. We normalize velocities to v_{te} eq. (16), times to τ_{te} eq. (17), the electron density to n_e , the electron distribution to n_e/v_{te}^3 , the quasilinear diffusion coefficient to $v_{te}^2\nu_{te}$, the electric field to $m_e v_{te} \nu_{te} / q_e$, the current density to $n_e q_e v_{te}$, power density to $n_e m_e v_{te}^2 \nu_{te}$, etc.

These normalizations coincide with those used by Kulsrud *et al.*⁵ However, they differ from those used in some of our earlier papers, e.g., ref. 6. (The thermal collision time differs by a factor of two.)

Since we are only dealing with the electron distribution, we will drop the species label from f and other electron quantities. Otherwise, we shall use the same notation for normalized and unnormalized quantities. For example, the electron Maxwellian eq. (18) reads in normalized terms

$$f_m(v) = \frac{1}{(2\pi)^{3/2}} \exp\left(-\frac{1}{2}v^2\right).$$

The reduction in the number of parameters now becomes apparent. The plasma is characterized by a single parameter Z_i and the quasilinear diffusion coefficient by three parameters D_0 , v_1 , and v_2 .

C. The numerical grid

We wish to solve eq. (1) in the domain V eq. (48). We do this by converting the differential equation to an algebraic equation using the finite difference method. In this method f is represented by its values on finite set of points and differentials are represented by differences between neighboring values.

First, we establish a numerical grid by dividing v and θ into N and M equal pieces, respectively. Thus we define

$$\Delta v = v_{\max}/N, \quad \Delta\theta = \pi/M, \quad (54)$$

together with grid positions

$$v_j = j \Delta v, \quad (55a)$$

$$\theta_i = i \Delta\theta. \quad (55b)$$

This grid system defines a system of cells. The electron distribution function is represented by its values at the *centers* of these cells, i.e., by the values

$$f_{i+1/2,j+1/2} = f(v_{j+1/2}, \theta_{i+1/2}), \quad \text{for } 0 \leq i < M, \quad 0 \leq j < N,$$

with i and j being integers; see fig. 3. The cell $v_j < v < v_{j+1}$, $\theta_i < \theta < \theta_{i+1}$ (i and j integers) is assigned a volume

$$V_{i+1/2,j+1/2} = 2\pi \sin \theta_{i+1/2} v_{j+1/2}^2 \Delta v \Delta\theta. \quad (56)$$

We will define numerical volume integration by

$$\text{int } X = \sum_{i=0}^{M-1} \sum_{j=0}^{N-1} X_{i+1/2,j+1/2} f_{i+1/2,j+1/2} V_{i+1/2,j+1/2}. \quad (57)$$

This is the discrete analogue of $\int_V X f d^3\mathbf{v}$; see eq. (13). We define the flux of a quantity through the boundary by

$$\text{flux } X = \sum_{i=0}^{M-1} 2\pi \sin \theta_{i+1/2} v_N^2 X_{i+1/2,N+1/2} S_{v,i+1/2,N} \Delta\theta, \quad (58)$$

which is a discrete analogue of $\int_A X \mathbf{S} \cdot d^2\mathbf{A}$. The number density of electrons becomes

$$n = \text{int } 1. \quad (59)$$

An alternative approach to finite differences is provided by the finite-element method where the f is represented by the superposition of a set of trial functions with finite support. This approach has been used in Fokker–Planck codes by workers at Lausanne.^{27,28} The finite-element method is also used in some commercial computer codes for the solution of partial differential equations. One such code has been applied to the Fokker–Planck equation by Fuchs *et al.*²⁹ If we identify the weights of the trial functions with the values of f at the grid positions, we see that the finite-difference and finite-element methods are quite similar. In particular, the goals of the methods are identical: to express algebraically $\partial f/\partial t$ at a particular location in terms of f at the same and neighboring locations (usually, the eight nearest neighbors). Thus our discussion of the time advancement of the equation in sec. VIII is independent of the choice of method.

D. Divergence of flux

Consider the Fokker–Planck equation in the form eq. (2). This is translated onto our numerical grid in a conservative form as

$$\frac{\partial f_{i+1/2,j+1/2}}{\partial t} = - \left(\frac{v_{j+1}^2 S_{v,i+1/2,j+1} - v_j^2 S_{v,i+1/2,j}}{v_{j+1/2}^2 \Delta v} + \frac{\sin \theta_{i+1} S_{\theta,i+1,j+1/2} - \sin \theta_i S_{\theta,i,j+1/2}}{v_{j+1/2} \sin \theta_{i+1/2} \Delta \theta} \right). \quad (60)$$

Notice that the fluxes are required on the edges of the cells (see fig. 3) and that the fluxes on the internal boundaries do not contribute since they are multiplied by $v_0 = 0$ or $\sin \theta_0 = \sin \theta_M = 0$. With this method we difference the fluxes and not the diffusion and friction coefficients. This lets us treat problems in which \mathbf{D}_w is discontinuous, e.g., as given by eqs. (46). The scheme in eq. (60) is accurate to second order in Δv and $\Delta \theta$.

This form of difference equation is called conservative because it obeys the conservation law

$$\frac{\partial \text{int } 1}{\partial t} + \text{flux } 1 = 0, \quad (61)$$

where int and flux are defined by eqs. (57) and (58). This is a discrete counterpart of eq. (5a). If $S_{v,i+1/2,N} = 0$ for all i , then we have flux 1 = 0 and particles are exactly conserved in the numerical scheme (if we ignore round-off errors). The discrete form of the parallel component of the momentum conservation law eq. (5b) is

$$\begin{aligned} \frac{\partial \text{int}(v \cos \theta)}{\partial t} + \text{flux}(v \cos \theta) &= \sum_{i=0}^{M-1} \sum_{j=0}^N 2\pi v_j^2 \sin \theta_{i+1/2} \cos \theta_{i+1/2} S_{v,i+1/2,j} \Delta v \Delta \theta \\ &\quad - \sum_{i=0}^M \sum_{j=0}^{N-1} 2\pi v_{j+1/2}^2 \sin^2 \theta_i S_{\theta,i,j+1/2} \Delta v 2 \sin(\frac{1}{2} \Delta \theta), \end{aligned} \quad (62)$$

while the energy conservation relation eq. (5c) becomes

$$\frac{\partial \text{int}(\frac{1}{2} v^2)}{\partial t} + \text{flux}(\frac{1}{2} v^2) = \sum_{i=0}^{M-1} \sum_{j=0}^N 2\pi \sin \theta_{i+1/2} v_j^3 S_{v,i+1/2,j} \Delta v \Delta \theta. \quad (63)$$

These relations are useful in that they establish definitions of various physical quantities that are consistent with the numerical scheme. For example, we can interpret the right-hand side of eq. (63) as the total power flowing into the electrons. This definition is consistent with the numerical definition of the energy of the electrons, namely $\text{int}(\frac{1}{2} v^2)$. Furthermore, we can determine the power flowing into the electrons from the waves (for example) by replacing S_v in the right-hand side of this equation by the flux due to the waves S_{wv} [compare with eq. (20)]. In this way, we obtain a complete and accurate power balance for the electrons. Similarly, the right-hand side of eq. (62) gives the definition of the force on the electrons. This is used when evaluating $P_{\parallel}^{e/e}$ in eq. (39).

[In order to prove eqs. (62) and (63), the following relation is useful:

$$\sum_{i=0}^{M-1} \frac{1}{2} (A_{i+1} + A_i) (B_{i+1} - B_i) = A_M B_M - A_0 B_0 - \sum_{i=0}^{M-1} \frac{1}{2} (B_{i+1} + B_i) (A_{i+1} - A_i).$$

This is the rule for “summing by parts”—the discrete counterpart of integration by parts.]

The basic difference equation (60) is readily generalized to nonuniform grids. However, the derivation of eqs. (62) and (63) relies on the uniformity of the grid and they cannot easily be generalized. Nonuniform spacing is used in FPPAC.⁴

E. Stream function

A very useful tool for understanding the Fokker–Planck equation (2) is the flux plot, which shows the vector field $\mathbf{S}(\mathbf{v})$. This is sometimes displayed as a set of arrows, one at each grid point, which point in the direction of \mathbf{S} and which have a length proportional to S . In this problem, S_v and S_θ are known at different locations, so that realization of this prescription would necessitate interpolation. Furthermore, such a display is often very misleading because the visual impression is strongly affected by whether the arrows line up with other grid points or not—a purely artificial aspect of the problem.

The much superior method is possible if we restrict ourselves to the steady state. In this case, the vector field $\mathbf{S}(\mathbf{v})$ is divergence-free $\nabla \cdot \mathbf{S} = 0$, and so may be expressed as the curl of a stream function, i.e.,

$$\mathbf{S}(\mathbf{v}) = \nabla \times \frac{nA(\mathbf{v})\hat{\phi}}{2\pi v \sin \theta},$$

where ϕ is the azimuthal coordinate. The components of \mathbf{S} are given by

$$S_v = \frac{n}{2\pi v^2 \sin \theta} \frac{\partial A}{\partial \theta}, \quad (64a)$$

$$S_\theta = -\frac{n}{2\pi v \sin \theta} \frac{\partial A}{\partial v}. \quad (64b)$$

Because $\mathbf{S} \cdot \nabla A = 0$, lines of constant A are stream lines. Thus a contour plot of $A(\mathbf{v})$ gives the vector field of $\mathbf{S}(\mathbf{v})$. The stream lines are obviously closed (indicating that the flow is divergence-free), and the total flux of electrons between any two contours is equal to the difference in the values of nA on those two contours.

We can compute A on the numerical grid using discrete analogs of eqs. (64)

$$A_{i,j} = \frac{2\pi v_j^2}{n} \sum_{i'=0}^{i-1} \sin \theta_{i'+1/2} S_{v,i'+1/2,j} \Delta \theta, \quad (65a)$$

$$= -\frac{2\pi \sin \theta_i}{n} \sum_{j'=0}^{j-1} v_{j'+1/2} S_{\theta,i,j'+1/2} \Delta v. \quad (65b)$$

If $\partial f_{i+1/2,j+1/2}/\partial t = 0$ according to eq. (60), then these two definitions are consistent.

F. Computation of the flux

In order to complete the specification of the difference scheme we must give formulas for $S_{v,i+1/2,j}$ and $S_{\theta,i,j+1/2}$ in eq. (60). These depend on the type of electron-electron collision operator used. We start with collisions off a Maxwellian background $C_{\text{Max}}^{e/e}$, eq. (41). This is the simplest case and yet it exhibits all the difficulties of solving the Fokker–Planck equation.

The collisional flux is given by the sum of the flux contributing to $C_{\text{Max}}^{e/e}$ which is given by eqs. (26) and (30) and the flux contributing to $C^{e/i}$ which is given by eqs. (26) and (36). [In fact, we compute the electron-electron flux by numerically evaluating the integrals in eqs. (27).] To this is added the quasilinear flux from eqs. (42) and (46) and the electric-field-induced flux from eq. (4). Both these terms are converted into spherical coordinates using eqs. (10). The total flux is then given by the general equations (9b) and (9c).

The diffusion and friction coefficients are computed at the points at which we need to know S_v and S_θ . Thus we compute $D_{vv,i+1/2,j}$, $D_{v\theta,i+1/2,j}$, $F_{v,i+1/2,j}$, and $D_{\theta v,i,j+1/2}$, $D_{\theta\theta,i,j+1/2}$, $F_{\theta,i,j+1/2}$.

The coefficients for S_v are not required at $j = 0$, nor those for S_θ at $i = 0, M$, because these fluxes are multiplied by zero in eq. (60). The boundary conditions eqs. (53) at v_{\max} are handled by setting

$$\begin{aligned} D_{vv,i+1/2,N} &\leftarrow 0, \\ D_{v\theta,i+1/2,N} &\leftarrow 0, \\ F_{v,i+1/2,N} &\leftarrow \max(F_{v,i+1/2,N}, 0). \end{aligned}$$

Next we must specify the way in which f and its derivatives are to be computed at the edges of the cells—i.e., locations $(i + 1/2, j)$ and $(i, j + 1/2)$ —in terms of the values of f at the centers of the cells $(i + 1/2, j + 1/2)$. Two of the terms are straightforward:

$$\frac{\partial f_{i+1/2,j}}{\partial v} = \frac{f_{i+1/2,j+1/2} - f_{i+1/2,j-1/2}}{\Delta v}, \quad (66a)$$

$$\frac{\partial f_{i,j+1/2}}{\partial \theta} = \frac{f_{i+1/2,j+1/2} - f_{i-1/2,j+1/2}}{\Delta \theta}. \quad (66b)$$

Again these expressions are accurate to second order.

The evaluation of f at the cell edges uses a method proposed by Chang and Cooper³⁰ extended here to two dimensions. The simple method, i.e.,

$$f_{i+1/2,j} = \frac{1}{2}(f_{i+1/2,j+1/2} + f_{i+1/2,j-1/2}),$$

turns out to give poor results for the steady-state distribution. Chang and Cooper replace this with

$$f_{i+1/2,j} = (1 - \delta_{i+1/2,j})f_{i+1/2,j+1/2} + \delta_{i+1/2,j}f_{i+1/2,j-1/2}, \quad (67a)$$

$$f_{i,j+1/2} = (1 - \delta_{i,j+1/2})f_{i+1/2,j+1/2} + \delta_{i,j+1/2}f_{i-1/2,j+1/2}, \quad (67b)$$

where the δ s are given by

$$\delta_{i+1/2,j} = g(-\Delta v F_{v,i+1/2,j} / D_{vv,i+1/2,j}), \quad (68a)$$

$$\delta_{i,j+1/2} = g(-\Delta \theta F_{\theta,i,j+1/2} / D_{\theta\theta,i,j+1/2}), \quad (68b)$$

and

$$g(w) = \frac{1}{w} - \frac{1}{\exp(w) - 1}. \quad (69)$$

The role of the δ is to weight the averaging performed in eqs. (67). The weighting is needed because often f is a strongly (exponentially) varying function of \mathbf{v} . An acute example of this is the Maxwellian distribution which varies very strongly for large v . In fact, the weighting is such that a Maxwellian is an exact steady-state solution when there is no rf and no electric field and when $C_{\text{Max}}^{e/e}$ is employed as the electron-electron collision operator. This is easily seen because for any isotropic distribution $S_{c\theta} = 0$; in that case, we also require $S_{cv} = 0$ in the steady state (because there are no sources or sinks of electrons). Using eqs. (26a) (with $a = b = e$), (66a), and (67a), together with $F_{cv,i+1/2,j}^{e/e} / D_{cv,i+1/2,j}^{e/e} = -v_j$, we find

$$\frac{f_{i+1/2,j+1/2}}{f_{i+1/2,j-1/2}} = \frac{f_{m,j+1/2}}{f_{m,j-1/2}} = \exp(-v_j \Delta v).$$

The errors in various moments of f are, therefore, exponentially small. With one-dimensional equations the weighting cures the problem of f becoming negative.³⁰ With our two-dimensional equation, this problem is alleviated but not cured. In general, this problem is solved by taking a sufficiently fine mesh (assuming that the electron-electron collision operator preserves the non-negative nature of f).

The function g has the properties

$$\begin{aligned} g(w) &= 1 - g(-w), \\ g(w) &= \frac{1}{2} - \frac{w}{12} + \frac{w^3}{720} + \dots, \\ g(-\infty) &= 1, \quad g(0) = \frac{1}{2}, \quad g(\infty) = 0. \end{aligned}$$

The first two properties are useful for evaluating $g(w)$ for $w \gg 1$ and $w \approx 0$, respectively.

The values of the cross-derivative terms which multiply the off-diagonal terms in the diffusion tensor ($D_{v\theta}$ and $D_{\theta v}$) are now given in terms of eqs. (67) as

$$\frac{\partial f_{i+1/2,j}}{\partial \theta} = \frac{f_{i+3/2,j} - f_{i-1/2,j}}{2\Delta\theta}, \quad (70a)$$

$$\frac{\partial f_{i,j+1/2}}{\partial v} = \frac{f_{i,j+3/2} - f_{i,j-1/2}}{2\Delta v}. \quad (70b)$$

The internal boundary conditions eqs. (50) give the values of $f_{i+1/2,j+1/2}$ beyond the internal boundaries as

$$\begin{aligned} f_{i+1/2,-1/2} &= f_{M-i-1/2,1/2}, \\ f_{-1/2,j+1/2} &= f_{1/2,j+1/2}, \\ f_{M+1/2,j+1/2} &= f_{M-1/2,j+1/2}. \end{aligned}$$

These conditions are only needed in the evaluation of cross-derivative terms. The form of eq. (60) automatically takes care of the internal boundaries for the other terms.

The external boundary at $v = v_{\max}$ is treated as follows: In the computation of $S_{v,i+1/2,N}$ we need only worry about the friction term (since $D_{vv} = D_{v\theta} = 0$ on the boundary) so that only $f_{i+1/2,N}$ is needed. Furthermore, the friction coefficient $F_{v,i+1/2,N}$ is non-negative. From eq. (67a), we have $f_{i+1/2,N} = f_{i+1/2,N-1/2}$ because $\delta_{i+1/2,N} \rightarrow 1$ for $F_{v,i+1/2,N} > 0$ and $D_{vv,i+1/2,N} = 0+$. (Obviously the value of $f_{i+1/2,N}$ is not required where $F_{v,i+1/2,N} = 0$.) Recall that the equation reduces to hyperbolic type on this boundary, so that no boundary condition should need to be specified here, as indeed is the case. In fact, the method reduces to the standard upstream differencing for a hyperbolic equation on this boundary. In the computation of $S_{\theta,i,N-1/2}$, only the cross-derivative term $\partial f_{i,N-1/2}/\partial v$ potentially involves points outside the integration domain. In this term, we use

$$\frac{\partial f_{i,N-1/2}}{\partial v} = \frac{f_{i,N-1/2} - f_{i,N-3/2}}{\Delta v},$$

instead of eq. (70b).

G. Matrix formulation

For collisions off a Maxwellian background the problem is *linear* so that eq. (60) can be rewritten as

$$\frac{\partial f}{\partial t} + Af = h, \quad (71)$$

where f is a vector of length MN of the values $f_{i+1/2,j+1/2}$ and A is an $MN \times MN$ matrix of coefficients. The right-hand side h (also a vector of length MN) is inserted to aid in the treatment of other collision operators. For the Maxwellian collision operator, we have $h = 0$. It is convenient to split A into three pieces, namely

$$A = A_v + A_\theta + A_\times,$$

where A_v contains the terms proportional to D_{vv} and F_v , A_θ contains those proportional to $D_{\theta\theta}$ and F_θ , and A_\times contains the cross-derivative terms proportional to $D_{v\theta}$ and $D_{\theta v}$. With the difference scheme given in this section A_v and A_θ are tridiagonal matrices. Thus we can write

$$(A_v f)_{i+1/2,j+1/2} = a_{v,i+1/2,j+1/2} f_{i+1/2,j-1/2} + b_{v,i+1/2,j+1/2} f_{i+1/2,j+1/2} + c_{v,i+1/2,j+1/2} f_{i+1/2,j+3/2}, \quad (72a)$$

$$(A_\theta f)_{i+1/2,j+1/2} = a_{\theta,i+1/2,j+1/2} f_{i-1/2,j+1/2} + b_{\theta,i+1/2,j+1/2} f_{i+1/2,j+1/2} + c_{\theta,i+1/2,j+1/2} f_{i+3/2,j+1/2}, \quad (72b)$$

where

$$a_{v,i+1/2,j+1/2} = \frac{v_j^2}{B_v} \left(-\frac{D_{vv,i+1/2,j}}{\Delta v} - F_{v,i+1/2,j} \delta_{i+1/2,j} \right), \quad (73a)$$

$$b_{v,i+1/2,j+1/2} = \frac{v_j^2}{B_v} \left(\frac{D_{vv,i+1/2,j}}{\Delta v} - F_{v,i+1/2,j} \epsilon_{i+1/2,j} \right) + \frac{v_{j+1}^2}{B_v} \left(\frac{D_{vv,i+1/2,j+1}}{\Delta v} + F_{v,i+1/2,j+1} \delta_{i+1/2,j+1} \right), \quad (73b)$$

$$c_{v,i+1/2,j+1/2} = \frac{v_{j+1}^2}{B_v} \left(-\frac{D_{vv,i+1/2,j+1}}{\Delta v} + F_{v,i+1/2,j+1} \epsilon_{i+1/2,j+1} \right), \quad (73c)$$

$$a_{\theta,i+1/2,j+1/2} = \frac{\sin \theta_i}{B_\theta} \left(-\frac{D_{\theta\theta,i,j+1/2}}{v_{j+1/2} \Delta \theta} - F_{\theta,i,j+1/2} \delta_{i,j+1/2} \right), \quad (73d)$$

$$b_{\theta,i+1/2,j+1/2} = \frac{\sin \theta_i}{B_\theta} \left(\frac{D_{\theta\theta,i,j+1/2}}{v_{j+1/2} \Delta \theta} - F_{\theta,i,j+1/2} \epsilon_{i,j+1/2} \right) + \frac{\sin \theta_{i+1}}{B_\theta} \left(\frac{D_{\theta\theta,i+1,j+1/2}}{v_{j+1/2} \Delta \theta} + F_{\theta,i+1,j+1/2} \delta_{i,j+1/2} \right), \quad (73e)$$

$$c_{\theta,i+1/2,j+1/2} = \frac{\sin \theta_{i+1}}{B_\theta} \left(-\frac{D_{\theta\theta,i+1,j+1/2}}{v_{j+1/2} \Delta \theta} + F_{\theta,i+1,j+1/2} \epsilon_{i,j+1/2} \right), \quad (73f)$$

where $\epsilon = 1 - \delta$, $B_v = \Delta v v_{j+1/2}^2$, and $B_\theta = v_{j+1/2} \Delta \theta \sin \theta_{i+1/2}$. With these coefficients the boundary conditions are reflected in the relations $a_{v,i+1/2,1/2} = c_{v,i+1/2,N-1/2} = 0$ and $a_{\theta,1/2,j+1/2} = c_{\theta,N-1/2,j+1/2} = 0$, which are automatically satisfied.

The matrix A_\times is more complicated with $(A_\times f)_{i+1/2,j+1/2}$ depending, in general, on the eight nearest neighbors to $f_{i+1/2,j+1/2}$. The boundary conditions have to be explicitly included in this matrix. We do not give expressions for the components of A_\times here because only the product $A_\times f$ is ever needed in the calculation. This is most easily computed directly in terms of the flux; this also cuts down on the storage requirements.

H. Alternate collision operators

The methods we will describe in the next sections for solving eq. (71) depend on the linearity of this equation and the fact that A_v and A_θ are tridiagonal matrices. With more complicated electron-electron collision operators, these conditions no longer hold. However, the techniques can still be used because the difference between the other collision terms and the Maxwellian collision term varies slowly in time.

If the full electron-electron collision operator is used, the basic framework given above still applies, except that the diffusion and friction coefficients $\mathbf{D}_c^{e/e}$ and $\mathbf{F}_c^{e/e}$ are now given in terms of gradients of the Rosenbluth potentials eqs. (24). These coefficients depend on f making the equation nonlinear. In

practice, the dependence on f is weak so that the coefficients only need to be recomputed occasionally. This also means that the equation is approximately linear so that the linear matrix techniques used to advance the equation in time still apply.

If the linearized or truncated collision operators are used, then the equation remains linear but with a term which involves an integral over f , namely $C(f_m(v), f(\mathbf{v}))$ or the truncation of this term. Again, this term is weakly dependent on f so that it need not be recomputed every time step. It is then most convenient to regard this term as the inhomogeneous driving term h eq. (71). For the truncated collision operator $C_{\text{trunc}}^{e/e}$, eq. (38), the elements of h are given by $C(f_m(v), f^{(1)}(v) \cos \theta)$ evaluated at $(v_{j+1/2}, \theta_{i+1/2})$. The computation of this term is described in appendix A.

VIII. Time Differencing

A. Crank–Nicholson method

We now turn to the method for advancing the Fokker–Planck equation in time. If the time step is Δt , then we define

$$f^k = f(t = t_k), \quad t_k = k\Delta t. \quad (74)$$

The simplest way of advancing eq. (71) is the explicit scheme

$$\frac{f^{k+1} - f^k}{\Delta t} + Af^k = h.$$

This is only accurate to first order in Δt . Furthermore, Δt must be chosen to be very small, on the order of Δv^2 or $\Delta \theta^2$, for stability. These defects are easily remedied by the Crank–Nicholson scheme³¹ which reads

$$\frac{f^{k+1} - f^k}{\Delta t} + A \frac{f^{k+1} + f^k}{2} = h. \quad (75)$$

This scheme is accurate to second order in Δt and is stable if A is positive definite. (This is a condition possessed by the continuous form of the operator A .) In order to solve eq. (75) for f^{k+1} we have to compute the inverse of $(I + \frac{1}{2}\Delta t A)$. This is a large banded matrix which can either be inverted using iterative methods or using Gaussian elimination. In both cases the number of operations is $O(N^3)$, (assuming $M \sim N$) making it a very expensive proposition. (This approach is discussed further in sec. IX.)

B. Alternating-direction-implicit method

Although $(I + \frac{1}{2}\Delta t A)$ is difficult to invert, the matrices $(I + \frac{1}{2}\Delta t A_v)$ and $(I + \frac{1}{2}\Delta t A_\theta)$ are rather easily inverted. This allows the *alternating-direction-implicit* method³¹ to be used. Unfortunately, $(I + \frac{1}{2}\Delta t A_\times)$ is not easily inverted and this means that the cross-derivative terms are treated explicitly in this method. Consider the equation

$$\left(I + \frac{\Delta t}{2}A_v\right)\left(I + \frac{\Delta t}{2}A_\theta\right)\frac{f^{k+1} - f^k}{\Delta t} + Af^k = h. \quad (76)$$

If we rearrange the terms in this equation to give

$$\left(I + \frac{\Delta t^2}{4}A_vA_\theta\right)\frac{f^{k+1} - f^k}{\Delta t} + (A_v + A_\theta)\frac{f^{k+1} + f^k}{2} + A_\times f^k = h,$$

we see that this method differs from the Crank–Nicholson method in two respects. Firstly, there is a Δt^2 term multiplying the time difference term. This difference is unimportant because it does not alter

the accuracy of the scheme. Secondly, the cross-derivative terms are treated explicitly. If we ignore the cross-derivative terms, eq. (76) is as accurate as the Crank–Nicholson scheme, but is much easier to realize because it is easy to solve eq. (76) for f^{k+1} . The explicit treatment of the cross-derivative terms lowers the accuracy and the stability, putting a limit on the maximum Δt that can be used. On the other hand, the implicit treatment of the other terms means that this method is far superior to the fully explicit method.

We can compute f^{k+1} from eq. (76) in a series of simple steps:

$$\begin{aligned}\phi^k &= h - Af^k, \\ \xi^{k+1/2} &= \left(I + \frac{\Delta t}{2} A_v \right)^{-1} \phi^k, \\ \xi^{k+1} &= \left(I + \frac{\Delta t}{2} A_\theta \right)^{-1} \xi^{k+1/2}, \\ f^{k+1} &= f^k + \Delta t \xi^{k+1}.\end{aligned}$$

The inversion of the matrices is carried out using Gaussian elimination as described in appendix A.

C. Example

Let us consider a specific example relevant to lower hybrid current drive. The plasma consists of electrons and infinitely massive ions with $Z_i = 1$. Electron-electron collisions are computed assuming a Maxwellian background using $C_{\text{Max}}^{e/e}$ eq. (41). Electron-ion collisions are given by eq. (37). The effect of the lower hybrid waves is modeled by a quasilinear diffusion coefficient given by eqs. (46) with $D_0 = 1$, $v_1 = 3$, and $v_2 = 5$. The electric field E is taken to be zero. Except for minor details this is the same example treated in the paper on lower hybrid current drive.⁶ (The time normalization used in that paper differs from the one adopted here by a factor of two.) We take $f(t = 0) = f_m$, $v_{\text{max}} = 10$, $M = N = 100$, and $\Delta t = 0.2$.

In studies of current drive, we are principally interested in the current density J , the rf power absorbed per unit volume by the plasma P , and their ratio J/P . These are defined by eqs. (19) and (20) whose discrete forms read

$$J = \frac{\text{int}(v \cos \theta)}{n}, \quad (77)$$

$$P = \frac{1}{n} \sum_{i=0}^{M-1} \sum_{j=0}^N 2\pi \sin \theta_{i+1/2} v_j^3 S_{wv, i+1/2, j} \Delta v \Delta \theta, \quad (78)$$

where n is given by eq. (59). (These definitions include a $1/n$ factor, because the n is included in the normalizations for J and P .)

The current is plotted as a function of time in fig. 4. With $\Delta t = 0.5$, the integration is unstable. The difference in the values of the current when the equations are integrated with $\Delta t = 0.2$ and $\Delta t = 0.05$ is about 0.1% of the final current.

The steady-state solution for f is shown in fig. 5. This may be obtained by integrating the equation sufficiently long (until about $t = 1000$) with a fixed time step or else using the techniques described in sec. IX. (With this numerical method, the steady state is independent of Δt .) The plateau in the resonant region is clearly visible as well as the considerable perpendicular heating. Using eqs. (77) and (78), we have $J = 5.754 \times 10^{-2}$, $P = 4.011 \times 10^{-3}$, and $J/P = 14.34$.

The flux plot for this case is given in fig. 6. This shows that the combination of rf diffusion and collisional scattering induces a perpendicular flux in the resonant region. Such flux plots are useful

in providing guidance for the analytic solution of this problem.²⁶ More extensive examination of this example can be found in the original paper⁶ including projections onto the v_{\parallel} axis, slices at constant v_{\perp} , etc.

There are two possible sources of error in these results: errors arising from the finite boundary (i.e., because v_{\max} is finite) and errors arising from the finite mesh. The effect of the boundary can be determined by increasing v_{\max} to 20 (and increasing N to 200). In the steady state, this gives $J = 5.759 \times 10^{-2}$, $P = 4.012 \times 10^{-3}$, $J/P = 14.35$ —changes of less than 0.1%. Thus for this particular problem, $v_{\max} = 10$ is adequate.

The effect of the discrete spatial grid is found by varying Δv and $\Delta\theta$. This we do by keeping $v_{\max} = 10$ varying M and N with $M = N$. Thus we have $N = 10/\Delta v$ and $\Delta\theta = \Delta v \pi/10$. The results for J and J/P are shown in fig. 7. We see that there is a lot of scatter in the data which arises because \mathbf{D}_w is discontinuous. As Δv and $\Delta\theta$ are varied, grid points (those on which the flux is defined) enter or leave the resonant region $v_1 < v_{\parallel} < v_2$. Each time this happens, there is a jump in J and P . As $\Delta v \rightarrow 0$, J approaches its asymptotic value of about 5.6×10^{-2} and the convergence to this value is as Δv . The finite mesh error in J with $M = N = 100$ is about 3%. This rate of convergence can be understood because J and P are exponentially dependent on v_1 [$J \sim \exp(-\frac{1}{2}v_1^2)$] and v_1 is determined only to within $\pm\frac{1}{2}\Delta v$. Thus the relative error in J and P is about $\exp(\frac{1}{2}v_1\Delta v) - 1 \approx \frac{1}{2}v_1\Delta v$. This gives a relative error of 15% for $v_1 = 3$, $N = 100$, $v_{\max} = 10$. The actual error is somewhat less than this because the boundary of the resonant region cuts across the grid lines and so v_1 is in fact determined more accurately than was assumed here. Because J and P are both subject to the same error, the ratio J/P is more accurately given: convergence to the asymptotic value of 14.24 is as Δv^2 and the value with $M = N = 100$ is in error by less than 1%.

If instead we use the truncated electron-electron collision operator $C_{\text{trunc}}^{e/e}$, the steady-state distribution function is rather similar to that shown in fig. 5. However, the flux plot fig. 8 shows a new eddy at low velocities due to the overall drift of the electrons with respect to the ions. (This plot is obtained with the same parameters as for fig. 6.) In this case, we find $J = 7.092 \times 10^{-2}$, $P = 4.294 \times 10^{-3}$, $J/P = 16.52$. The enhancement of the efficiency J/P comes about because momentum (and hence current) is no longer lost when tail electrons collide with bulk electrons.

A check on the implementation of the $C_{\text{trunc}}^{e/e}$ is given by measuring the electrical conductivity. For $Z_i = 1$, the exact conductivity is given by table I as $J/E = 7.429 \approx 0.582 \times 16\sqrt{2/\pi}$.²¹ Integrating the Fokker–Planck equation using the truncated collision operator with no rf $D_0 = 0$ and a small electric field $E = 10^{-3}$, the conductivity is $J/E = 7.446$, a 0.3% error. This small error is probably attributable partly to the finite mesh size (here we again took $M = N = 100$ and $v_{\max} = 10$) and partly to the finiteness of E (since there is a contribution to the current which varies as E^3). In contrast, if $C_{\text{Max}}^{e/e}$ is used the conductivity is $J/E = 3.772$ a factor of two too small.⁵

IX. Steady-State Solution

A. Statement of problem

Often, we are only interested in the steady-state solution to the Fokker–Planck equation. Nearly always we must resort to an iterative method for obtaining the steady state. In that case we need some measure of how close we are to the steady state so that iteration may be stopped when this is small enough. The measure we shall employ is

$$R = \frac{1}{n} \sqrt{\text{int} \left[\left(\frac{\partial f}{\partial t} \right)^2 \right]}, \quad (79)$$

where the *residue* $\partial f/\partial t$ is given by eq. (60). Somewhat arbitrarily we use $R = 10^{-9}$ as the convergence criterion.

One obvious way of obtaining a steady state is to integrate the time-dependent solution as described in sec. VIII for a long time. This should be done with the largest time step consistent with stability. For the example shown in fig. 5, the convergence criterion is met at time $t = 812$. The largest time step that can be used is approximately 0.2; so that 4060 steps are required. The CPU time required to run the Fokker–Planck code on the Cray–1 is approximately $2 \mu\text{s}$ per mesh point per time step. Thus, achieving the steady state by this method takes about 80 s. This is rather expensive and it is therefore desirable to find faster methods.

However, this method is quite effective when $A_x = 0$. Then the numerical scheme is stable even if Δt is large. For example, for the electric field example discussed in sec. VIII in which $D_0 = 0$ and $E = 10^{-3}$, we can take $\Delta t = 1$, and the convergence criterion is met after 220 steps. Here the integral portion of $C_{\text{trunc}}^{e/e}$, which is represented by the term h in eq. (71), is evaluated every tenth time step. The numerical method is stable for larger values of Δt . But, because the integration is less accurate, more steps are required to meet the convergence criterion. With large Δt the numerical solution tends to oscillate about the steady state.

B. Chebyshev acceleration

A significant improvement can be achieved by using a varying time step. Hewett *et al.*³² describe an adaptive time selection for the alternating direction implicit method which speeds the convergence by a factor of two to three. Here we describe Chebyshev acceleration³¹ which is a nonadaptive method for selecting varying time steps. We choose the time step $\Delta t_k = t_{k+1} - t_k$ according to

$$\Delta t_k = \frac{2}{\beta + \alpha - (\beta - \alpha) \cos\left(\frac{[2(k \bmod K) + 1]\pi}{2K}\right)}, \quad (80)$$

where α , β , and K are constants with $\alpha < \beta$ and $K = \text{integer}$. The advantage of this method is that by changing a few lines of code it can easily be incorporated into the alternating-direction-implicit method described in sec. VIII. A fixed time step is recovered in the special case $\alpha = \beta = 1/\Delta t$.

Let us discuss the choice of the parameters in eq. (80). With K large, eq. (80) gives a series of K time steps (repeated periodically) varying from $1/\alpha$ down to $1/\beta$. In the examples we consider, we take $K = 20$. Then the maximum time step is somewhat less than $1/\alpha$ while the minimum time step is very close to $1/\beta$. In order to realize performance gains with this method we wish to pick the minimum time step comfortably within the stability threshold for the fixed-time-step method, while the maximum time step is considerably greater than the stability threshold.

The method works because the long wavelength eigenmodes of the linear operator decay slowly but are stable with large Δt ; on the other hand, the short wavelength modes decay rapidly but are only stable if Δt is small. Consider a particular cycle of K steps. During the initial large time steps, the long wavelength modes are efficiently damped (because Δt is large), but the short wavelength modes grow. This is followed by successively shorter time steps which damp the short wavelength modes.

For the example shown in fig. 5, the stability threshold for Δt lies between 0.2 and 0.5. Thus we choose $1/\beta = 0.05$ and $1/\alpha = 1000$. With $K = 20$ this gives a maximum time step of 31.4, a minimum step of 0.05, and an average time step of 1.95. Since the average time step is about 10 times the largest time step that can be used in the fixed time step scheme, we expect convergence to be 10 times faster. Indeed this is the case. The convergence criterion is met after 400 steps at $t = 790$. This takes about 8 s of CPU time. The variation of R with time is shown in fig. 9. This shows the growth of R during the large time steps followed by a drop in R as the instabilities are quenched during the small time steps.

The overall decay of R with t closely matches that seen with a fixed time step. (This is contrary to the experience of Hewett *et al.* with their adaptive code in which the rates of decay are very different.³²)

C. Runaway problem

If the electric field is sufficiently large to produce runaways, i.e., $E > v_{\max}^{-2}$, then as $t \rightarrow \infty$ a steady state is reached which decays at the runaway rate γ (assuming that a linear collision operator is employed). Because f and all its moments decay at the same rate, γ is given from eq. (61) as

$$\gamma = \frac{\text{flux } 1}{\text{int } 1}, \quad (81)$$

which we will take to be the definition of γ for all t . Thus we write

$$f(v, t) = f'(v, t) \exp\left(-\int_0^t \gamma(t') dt'\right), \quad (82)$$

where γ is given by eq. (81) and $f'(t \rightarrow \infty)$ is independent of t . If eq. (82) is substituted into eq. (71), we obtain

$$\frac{\partial f'}{\partial t} + (A - \gamma)f' = 0, \quad (83)$$

where for simplicity we set the inhomogeneous term h to zero. Because γ is expressed as an integral over f eq. (81), it varies slowly and need not be evaluated very often. Thus eq. (83) may be regarded as a linear equation and solved in precisely the same way as eq. (71) (with $h = 0$) except that γ must be subtracted from $b_{v,i+1/2,j+1/2}$ eq. (73b).

As an example, fig. 10 shows the steady-state distribution obtained by this method with $Z_i = 1$, $E = 0.06$, $M = N = 100$, $v_{\max} = 10$, and electron-electron collisions given by $C_{\text{Max}}^{e/e}$. Since there is no rf diffusion term, there are no cross-derivative terms and the steady state is most easily obtained by taking a constant time step of $\Delta t = 1$. The runaway rate γ is recomputed every ten time steps and the convergence condition $R = 10^{-9}$ is met after 820 time steps. In the steady state, we have $\gamma = 5.211 \times 10^{-5}$ and $J = 0.3133$. These are close to the results obtained by Kulsrud *et al.*,⁵ namely $\gamma = 5.411 \times 10^{-5}$ and $J = 0.3143$.

Again, it is important to explore the possible errors in these figures. Extending the boundary to $v_{\max} = 20$ and doubling N to 200 gives $\gamma = 5.210 \times 10^{-5}$ and $J = 0.4514$. While there is practically no change in γ , J is about 50% larger. This discrepancy arises because there is a large contribution to the total current by the runaways in the region $10 < v < 20$. We can verify this by estimating the total current for an arbitrary v_{\max} on the basis of the results from $v_{\max} = 10$. For simplicity, assume that all the runaways are concentrated near $v_{\perp} = 0$. From small γ and in the limit $t \rightarrow \infty$, the runaway distribution is independent of v_{\parallel} , so that $f(v_{\parallel} \gg v_t) \approx (\gamma/E)\delta(v_{\perp})$. The current obtained by integrating $v_{\parallel}f$ out to $v = v_{\max}$ is then

$$J(v_{\max}) \approx J_{\text{bulk}} + \frac{1}{2}(\gamma/E)v_{\max}^2,$$

where, using the data from $v_{\max} = 10$, we have $J_{\text{bulk}} = 0.270$. We can interpret J_{bulk} as the current carried by the bulk electrons and the other term as the current carried by the runaways. This now gives $J(v_{\max} = 20) = 0.444$ which is within 2% of the observed value. The lesson from this exercise is that it makes little sense to quote the result for J when the runaway rate is appreciable because it depends strongly on v_{\max} . It is preferable to determine the bulk current since this is then weakly dependent on v_{\max} and has a physical interpretation. We have seen that $v_{\max} = 10$ is sufficiently large to give γ and J_{bulk} accurately.

In order to determine the effect of the finite mesh on the runaway results, we vary M and N with $M = N$ and $v_{\max} = 10$. The results for γ and J are shown in fig. 11. The asymptotic values are

$\gamma = 5.185 \times 10^{-5}$ and $J = 0.31334$. The errors in the values for $M = N = 100$ are 0.5% and 0.02%, respectively. The errors are considerably less than with the rf problem in fig. 7 and the convergence is much more regular (as Δv^2).

A disadvantage of solving for the decaying steady state of the distribution, eq. (83), is that \mathbf{S} is no longer divergence free. This means that the stream lines cannot be plotted as contours of a stream function A , eq. (65). This can be remedied by injecting electrons at the origin to match the runaway loss of particles. Although this is a rather artificial problem, there is little error in the runaway rate provided that the runaway rate itself is small. We implement this procedure as follows: The loss of particles at $v = v_{\max}$ is

$$n\gamma = \text{flux } 1.$$

We match this loss by a uniform radial flux at the origin

$$v_0^2 S_{v,i+1/2,0} = \frac{n\gamma \sin(\frac{1}{2}\Delta\theta)}{2\pi \Delta\theta},$$

which is chosen to give

$$\sum_{i=0}^{M-1} 2\pi \sin \theta_{i+1/2} v_0^2 S_{v,i+1/2,0} \Delta\theta = n\gamma.$$

(The product $v_0^2 S_{v,i+1/2,0}$ is finite even though $S_{v,i+1/2,0}$ is infinite.) From eq. (60), we see that this introduces a source term $v_0^2 S_{v,i+1/2,0} / (v_{1/2}^2 \Delta v)$ into the expressions for $\partial f_{i+1/2,1/2} / \partial t$. This is included as part of the inhomogeneous term h in eq. (71). The expressions for the stream function eqs. (65) require a slight modification to give

$$\begin{aligned} A_{i,j} &= -\gamma + \frac{2\pi v_j^2}{n} \sum_{i'=0}^{i-1} \sin \theta_{i'+1/2} S_{v,i'+1/2,j} \Delta\theta, \\ &= A_{i,0} - \frac{2\pi \sin \theta_i}{n} \sum_{j'=0}^{j-1} v_{j'+1/2} S_{\theta,i,j'+1/2} \Delta v, \end{aligned}$$

where the integration constant has been chosen to give $A_{0,j} = -\gamma$ and $A_{M,j} = 0$.

The flux plot computed by this method for the case shown in fig. 10, i.e., for $Z_i = 1$, $E = 0.06$, $M = N = 100$, $v_{\max} = 10$, is shown in fig. 12. When computed in this way, the runaway rate is slightly lower $\gamma = 5.148 \times 10^{-5}$ because a typical runaway particle has to be accelerated from $v = 0$ instead of $v = 1$. The current $J = 0.3127$ is also lower.

D. Other methods

An *infinite* time step can be used if the Crank–Nicholson scheme, eq. (75), is modified so that f^{k+1} is used in place of $\frac{1}{2}(f^{k+1} + f^k)$. Then, the steady state can be achieved in a single time step. Of course, this entails inverting the large matrix A (which is why we advocated using the alternating-direction-implicit method in preference to the Crank–Nicholson method). However, routines are available to perform such an inversion and they have been employed by O'Brien *et al.*³³ An important feature of this method is the use of disk files to hold intermediate results. (Typically, the full matrix cannot fit into memory.) They report a CPU time of 35 s to invert the matrix arising from the discretization of the Fokker–Planck equation on a 300×100 grid with this time scaling as $MN \times \min(M, N)$. This method is therefore comparable (as far as CPU time goes) to the Chebyshev acceleration method. There are two potential drawbacks of this scheme: Firstly, there is a significant cost in I/O time with this method because of the use of disk files for storage. Secondly, the advantage of the method is reduced if the steady state cannot

be reached in a single time step. This is the case with the more complicated collision operators, because the matrix A is a function of time.

Various iterative methods are available for obtaining a steady-state solution.³¹ These are basically approximate methods of inverting the matrix A . Notable is Gauss–Seidel relaxation in which the elements of f are successively updated to achieve $\partial f/\partial t = 0$ at the point in question. In line relaxation, a whole line of elements (for example, $j = \text{const}$) is updated simultaneously (requiring the solution of a tridiagonal system of equations). Line relaxation gives the same convergence rate as Gauss–Seidel relaxation and may be vectorized if the even-numbered rows ($j = \text{even}$) are updated in one sweep followed by the update on the odd-numbered rows.

The odd-even line relaxation method is extended with the successive-over-relaxation method where the over-relaxation parameter ω determines how much overshoot there is beyond the value of f which gives $\partial f/\partial t = 0$. Unfortunately, these methods give results which are roughly the same as using fixed time steps. For the example shown in fig. 5, with the over-relaxation parameter set to $\omega = 1.4$, the convergence criterion is met after 5980 steps. (Compare this to the 4060 steps required in the fixed-time-step method. However, one relaxation step tends to be computationally less expensive than one step of the alternating-direction-implicit method.) For this example, the method becomes unstable with $\omega \geq 1.5$.

Although by themselves relaxation methods are not very useful for this problem, they are an important ingredient in the multigrid method.^{34,35} In this method, the problem is solved at several different grid spacings (usually differing from each other by a factor of two). A few relaxation sweeps are carried out on the finest grid. Because relaxation is a local method, this is very effective at damping the short wavelength modes (with wavelength comparable to grid spacing). If relaxation is continued on the finest grid, convergence would become slower because longer wavelength modes would dominate the residue. However, in the multigrid method, the residue is transferred onto the next coarsest grid where relaxation methods are again efficient. This process continues recursively up to very coarse grids where either relaxation methods or direct solution methods can be used.

This method has not been implemented for the Fokker–Planck equation. However, we can estimate the time required to obtain a steady state. Each relaxation step on the finest grid gives a reduction in R by about a factor of two. (The total work at the coarser grids is at most a multiple of the work on the finest grid.) In contrast, the mean reduction in R with the Chebyshev method is by 4% per step (see fig. 9). Thus the multigrid method will require about $\log(0.5)/\log(0.96) \approx 16$ times fewer steps—an order-of-magnitude improvement over the Chebyshev method.

X. Relativistic Treatment

A. The Fokker–Planck equation

Fokker–Planck methods have been used to study current drive by lower hybrid waves. In a fusion plasma, these waves will interact with electrons that travel at close to the speed of light. In such cases, it is necessary to reformulate the equation to include relativistic effects. The first change is that the electron distribution function is expressed in momentum rather than velocity space so that eq. (1) becomes

$$\frac{\partial f_e}{\partial t} - \sum_s C(f_e, f_s) + \nabla \cdot \mathbf{S}_w + q_e \mathbf{E} \cdot \nabla f_e = 0, \quad (84)$$

where now the $\nabla \equiv \partial/\partial \mathbf{p}$ operator operates in *momentum* space, \mathbf{S}_w is the rf-induced flux in momentum space, and f_e is normalized so that

$$\int f_e(\mathbf{p}) d^3 \mathbf{p} = n_e.$$

In spherical coordinates we have

$$\nabla \cdot \mathbf{S} = \frac{1}{p^2} \frac{\partial}{\partial p} p^2 S_p + \frac{1}{p \sin \theta} \frac{\partial}{\partial \theta} \sin \theta S_\theta,$$

where $\cos \theta = p_{\parallel}/p$.

In addition, the forms of the collision term and the quasilinear diffusion term are altered.

B. The relativistic collision operator

The relativistic collision operator is given by Beliaev and Budker.³⁶ It can again be written as the divergence of a flux $C(f_a, f_b) = -\nabla \cdot \mathbf{S}_c^{a/b}$, where now we have

$$\mathbf{S}_c^{a/b} = \frac{q_a^2 q_b^2}{8\pi\epsilon_0^2} \ln \Lambda^{a/b} \int \mathbf{U}(\mathbf{u}) \cdot \left(f_a(\mathbf{p}) \frac{\partial f_b(\mathbf{p}')}{\partial \mathbf{p}'} - f_b(\mathbf{p}') \frac{\partial f_a(\mathbf{p})}{\partial \mathbf{p}} \right) d^3 \mathbf{p}'. \quad (85)$$

The expression for \mathbf{U} is rather complicated.³⁶ However, if either the test or the background species is weakly relativistic ($p \ll m_a c$ or $p' \ll m_b c$), then \mathbf{U} may be approximated by its nonrelativistic form

$$\mathbf{U}(\mathbf{u}) = \frac{u^2 \mathbf{I} - \mathbf{u}\mathbf{u}}{u^3}, \quad \mathbf{u} = \mathbf{v}_a - \mathbf{v}_b,$$

where $\mathbf{v}_s = \mathbf{p}/m_s \gamma_s$ is the velocity of species s , $\gamma_s = (1 + p^2/m_s^2 c^2)^{1/2}$ is the relativistic correction factor, and m_s is the rest mass.

Despite the resemblance of eq. (85) to eq. (21), this collision operator cannot be readily expressed in terms of Rosenbluth potentials. However, considerable progress can still be made by working directly with eq. (85). We restrict our attention to electron-ion and electron-electron collisions.

For collisions off infinitely massive ions, we can take the ions to be stationary $v_i' \rightarrow 0$ and evaluate the integrals to give

$$C^{e/i}(f_e(\mathbf{p})) = \Gamma^{e/e} \frac{Z_i}{2v_e p^2} \frac{1}{\sin \theta} \frac{\partial}{\partial \theta} \sin \theta \frac{\partial}{\partial \theta} f_e(\mathbf{v}), \quad (86)$$

where

$$\Gamma^{a/b} = \frac{n_b q_a^2 q_b^2 \ln \Lambda^{a/b}}{4\pi\epsilon_0^2}$$

(this differs by a factor of m_a^2 from the definition given in sec. II).

For electron-electron collisions we start with the case of an isotropic background $C(f_e(\mathbf{p}), f_e^{(0)}(p))$. The fluxes for this term are¹⁹

$$S_{cp}^{e/e} = -D_{cpp}^{e/e} \frac{\partial f_e}{\partial p} + F_{cp}^{e/e} f_e, \quad (87a)$$

$$S_{c\theta}^{e/e} = -D_{c\theta\theta}^{e/e} \frac{1}{p} \frac{\partial f_e}{\partial \theta}, \quad (87b)$$

where

$$D_{cpp}^{e/e} = \frac{4\pi\Gamma^{e/e}}{3n_e} \left(\int_0^p p'^2 f_e^{(0)}(p') \frac{v_e'^2}{v_e^3} dp' + \int_p^\infty p'^2 f_e^{(0)}(p') \frac{1}{v_e'} dp' \right), \quad (88a)$$

$$D_{c\theta\theta}^{e/e} = \frac{4\pi\Gamma^{e/e}}{3n_e} \left(\int_0^p p'^2 f_e^{(0)}(p') \frac{3v_e^2 - v_e'^2}{2v_e^3} dp' + \int_p^\infty p'^2 f_e^{(0)}(p') \frac{1}{v_e'} dp' \right), \quad (88b)$$

$$F_{cp}^{e/e} = -\frac{4\pi\Gamma^{e/e}}{3n_e} \left(\int_0^p p' f_e^{(0)}(p') \frac{3v_e' - v_e'^3/c^2}{v_e^2} dp' + \int_p^\infty p' f_e^{(0)}(p') 2v_e/c^2 dp' \right). \quad (88c)$$

These should be compared with their nonrelativistic counterparts eqs. (26) and (27).

In the relativistic limit, the Maxwellian distribution eq. (18) becomes³⁷

$$f_{em}(p) = \frac{n_e}{4\pi m_e^2 c T_e K_2(\Theta^{-1})} \exp\left(-\frac{\mathcal{E}}{T_e}\right), \quad (89)$$

where

$$\mathcal{E} = m_e c^2 \gamma_e$$

is the total electron energy,

$$\Theta = T_e / m_e c^2 = T_e / 511 \text{ keV},$$

and K_n is the n th-order modified Bessel function of the second kind. If we substitute $f_e^{(0)}(p) = f_{em}(p)$ into eqs. (88), we obtain $F_{cp}^{e/e} / D_{cpp}^{e/e} = -v_e / T_e$. Thus we find that f_{em} annihilates the electron-electron collision term $C(f_{em}, f_{em}) = 0$. The integrals in eq. (88) cannot be performed analytically with $f_e^{(0)}(p) = f_{em}(p)$ and so in the numerical code these are performed numerically.

For the Maxwellian distribution eq. (89), we define a thermal momentum

$$p_{te} = \sqrt{m_e T_e},$$

a thermal velocity

$$v_{te}^2 = \frac{1}{3n_e} \int v_e^2 f_{em}(p) d^3 \mathbf{p} = \frac{T_e}{m_e} \left(1 - \frac{5}{2} \Theta + \frac{55}{8} \Theta^2 + \dots\right),$$

and a thermal collision frequency

$$\nu_{te} = \frac{m_e \Gamma^{e/e}}{p_{te}^3}.$$

For $p \gg p_{te}$, the indefinite limits in the integrals in Eq. (88) can be replaced by ∞ , giving³⁸

$$D_{cpp}^{e/e} = \Gamma^{e/e} \frac{v_{te}^2}{v_e^3}, \quad (90a)$$

$$D_{c\theta\theta}^{e/e} = \Gamma^{e/e} \frac{1}{2v_e} \left(1 - \frac{v_{te}^2}{v_e^2}\right), \quad (90b)$$

$$F_{cp}^{e/e} = -\Gamma^{e/e} \frac{v_{te}^2}{T_e v_e^2}. \quad (90c)$$

These should be compared with eqs. (28).

For a background which consists of just the first Legendre harmonic, the collision term is $C(f_{em}(p), f_e^{(1)}(p) \cos \theta)$. This is given by¹⁹

$$\begin{aligned} \frac{C(f_{em}(p), f_e^{(1)}(p) \cos \theta)}{f_{em}(p) \cos \theta} &= \frac{4\pi \Gamma^{e/e}}{n_e} \times \\ &\left\{ \frac{m_e f_e^{(1)}(p)}{\gamma_e} + \frac{1}{5} \int_0^p p'^2 f_e^{(1)}(p') \frac{m_e}{T_e} \left[\frac{\gamma_e v_e'}{p'^2 \gamma_e'^3} \left(\frac{T_e}{m_e c^2} (4\gamma_e'^2 + 6) - \frac{1}{3} (4\gamma_e'^3 - 9\gamma_e') \right) \right. \right. \\ &\quad \left. \left. + \frac{\gamma_e^2 v_e'}{p'^2 \gamma_e'^3} \left(\frac{m_e v_e'^2}{T_e} \gamma_e'^3 - \frac{1}{3} (4\gamma_e'^2 + 6) \right) \right] dp' \right. \\ &\quad \left. + \frac{1}{5} \int_p^\infty p'^2 f_e^{(1)}(p') \frac{m_e}{T_e} \left[\frac{\gamma_e' v_e}{p'^2 \gamma_e^3} \left(\frac{T_e}{m_e c^2} (4\gamma_e^2 + 6) - \frac{1}{3} (4\gamma_e^3 - 9\gamma_e) \right) \right. \right. \\ &\quad \left. \left. + \frac{\gamma_e'^2 v_e}{p'^2 \gamma_e^3} \left(\frac{m_e v_e^2}{T_e} \gamma_e^3 - \frac{1}{3} (4\gamma_e^2 + 6) \right) \right] dp' \right\}. \quad (91) \end{aligned}$$

[Compare with eq. (34).] The general solution of the linearized electron-electron collision operator $C(f_e, f_{em}) + C(f_{em}, f_e) = 0$ is

$$f_e = (a + \mathbf{b} \cdot \mathbf{p} + d\mathcal{E})f_{em},$$

where a , \mathbf{b} , and d are arbitrary constants. With $a = d = 0$ and $\mathbf{b} = \hat{\mathbf{p}}_{\parallel}$, this provides a useful check on Eqs. (88) and (91) and their computational realizations.

In the example we show below, we use the electron-ion collision operator given by eq. (86) and the relativistic generalization of the truncated collision operator eq. (38)

$$C_{\text{trunc}}^{e/e}(f_e(\mathbf{p})) = C(f_e(\mathbf{p}), f_{em}(p)) + C(f_{em}(p), f_e^{(1)}(p) \cos \theta), \quad (92)$$

where the first term is given by eqs. (87) and (88) and the second term by eq. (91).

C. Wave-particle interaction

We saw in sec. V that the quasilinear diffusion operator had two principal ingredients: the wave-particle resonance condition, and the diffusion paths. Both of these are modified by relativistic effects.

The wave-particle resonance condition becomes

$$\omega - k_{\parallel} v_{e\parallel} - n\Omega_e/\gamma_e = 0,$$

where $\Omega_e = q_e B/m_e$ is the rest-mass cyclotron frequency. Translating this into momentum space gives

$$\omega \sqrt{1 + p^2/m_e^2 c^2} - k_{\parallel} p_{\parallel} - n\Omega_e = 0.$$

This modification of the resonance condition is important in the consideration of current drive by electron cyclotron waves.³⁹

The diffusion paths are again given by surfaces of constant energy in the wave frame. The expression for the energy in a frame moving at $(\omega/k_{\parallel})\hat{\mathbf{p}}_{\parallel}$ is

$$\mathcal{E}' = \frac{\mathcal{E} - (\omega/k_{\parallel})p_{\parallel}}{\sqrt{1 - \omega^2/k_{\parallel}^2 c^2}}.$$

The diffusion paths are, therefore, given by

$$\mathcal{E} - (\omega/k_{\parallel})p_{\parallel} = \text{const.}$$

These paths are parallel to the vector

$$\left(\frac{\omega}{k_{\parallel}} - v_{e\parallel} \right) \hat{\mathbf{p}}_{\perp} + v_{e\perp} \hat{\mathbf{p}}_{\parallel}.$$

This should be compared with the vector \mathbf{a}_n defined in sec. V. The paths are ellipses or hyperbolae in momentum space depending on whether ω/k_{\parallel} is less than or greater than c .²⁵

For lower hybrid waves, we have $n = 0$ and the diffusion is in the parallel direction. We, therefore, generalize eqs. (46) by incorporating the modified resonance condition to read

$$\mathbf{D}_w = D_w(p_{\perp}, p_{\parallel}) \hat{\mathbf{p}}_{\parallel} \hat{\mathbf{p}}_{\parallel}, \quad (93a)$$

where

$$D_w(p_{\perp}, p_{\parallel}) = \begin{cases} D_0, & \text{for } v_1 < p_{\parallel}/\gamma_e < v_2, \\ 0, & \text{otherwise.} \end{cases} \quad (93b)$$

D. Example

To illustrate the relativistic effects we show in fig. 13 the steady-state distribution function obtained by integrating the Fokker–Planck equation with electron–electron collisions given by $C_{\text{trunc}}^{e/e}$ eq. (92) and electron–ion collisions given by $C^{e/i}$ eq. (86) with $Z_i = 1$. The quasilinear diffusion term is given by eq. (93) with $D_0 = 1$, $v_1 = 0.4c$, and $v_2 = 0.7c$. (Except for the perpendicular profile of \mathbf{D}_w , this is the same as the example given in ref. 19.) The integration is carried out with $M = N = 100$ and $p_{\text{max}} = 20$. We normalize all momenta to p_{te} , velocities to p_{te}/m_e (not v_{te}), the current density to $n_e q_e p_{te}/m_e$, the power density to $n_e p_{te}^2 v_{te}/m_e$, etc. Again we are principally interested in the current and the power dissipated. These are defined by

$$J = \frac{\text{int}(v_e \cos \theta)}{n},$$

$$P = \frac{1}{n} \sum_{i=0}^{M-1} \sum_{j=0}^N 2\pi \sin \theta_{i+1/2} v_j p_j^2 S_{wp,i+1/2,j} \Delta p \Delta \theta,$$

where int is the generalization of eq. (57) to momentum space, $n = \text{int } 1$. [Compare these expressions with eqs. (77) and (78).] In the steady state, we find $J = 3.732 \times 10^{-3}$, $P = 1.256 \times 10^{-4}$, and $J/P = 29.72$.

Again a useful benchmark is provided by the electrical conductivity. In the limit $E \rightarrow 0$ this is correctly given if $C_{\text{trunc}}^{e/e}$ is employed. With $E = 10^{-3}$, $Z_i = 1$, $\Theta = 0.01$, $M = N = 100$, and $p_{\text{max}} = 10$, we find $J/E = 7.307$, which differs from the true value of 7.291 by about 0.2%. Values of the conductivity for various values of Z_i and Θ are tabulated in table II.

XI. Adjoint Method

A. Introduction and example

We have considered here techniques for solving the Fokker–Planck equation with an added quasilinear diffusion term. This tends to be an expensive operation because the addition of the quasilinear diffusion term greatly increases the parameter space to be scanned. For example, the study of lower hybrid current drive⁶ included the results of some 50 runs with different values of v_1 and v_2 . Even so, no systematic study was made of the dependence on the parameters D_0 and Z_i .

However, the amount of work can be drastically reduced using the adjoint method. This was introduced by Hirshman⁴⁰ for the study of beam-driven currents. Later, Antonsen and Chu⁴¹ used it to study rf-driven currents.

To illustrate the method, we will outline the analysis given by Antonsen and Chu.⁴¹ The method begins by assuming that f_e is close to a Maxwellian f_{em} so that the linearized electron–electron collision operator $C_{\text{lin}}^{e/e}$ eq. (31) can be used. The quasilinear diffusion term is taken as a *given*. As pointed out in sec. V, the Fokker–Planck equation then becomes an inhomogeneous equation, whose linear operator is independent of the wave drive. Two further assumptions are made, namely that $\mathbf{E} = 0$ and that a steady state has been reached. (Neither of these assumptions is necessary and they have been relaxed in ref. 42.) The Fokker–Planck equation is then

$$C(f_e(\mathbf{v})) \equiv C_{\text{lin}}^{e/e}(f_e(\mathbf{v})) + C^{e/i}(f_e(\mathbf{v}))$$

$$= \nabla \cdot \mathbf{S}_w + \left(\frac{m_e v^2}{2T_e} - \frac{3}{2} \right) f_{em}(v) \frac{\partial \ln T_e}{\partial t}, \quad (94)$$

where we have inserted the Chapman–Enskog–Braginskii energy loss term to ensure that eq. (94) has a solution (i.e., to ensure that the Fokker–Planck equation reaches a steady state). Taking the energy moment of this equation, and noting that the collision operator is energy conserving, we find the equation for $\partial T_e/\partial t$

$$\frac{\partial}{\partial t} \left(\frac{3}{2} n_e T_e \right) = P,$$

where P is given by eq. (20).

The straightforward approach is now to solve eq. (94) for a particular \mathbf{S}_w , determine the electron distribution f_e , and hence find the rf-driven current. The adjoint method gives a way of computing the current without having to find f_e . Consider first the “adjoint” problem

$$C(f_{em}(v)\chi(\mathbf{v})) = -q_e v_{\parallel} f_{em}(v), \quad (95)$$

where we require that $f_{em}\chi$ have zero density and zero energy. This is the Spitzer–Härm equation for the perturbed distribution in the presence of an electric field $\mathbf{E} = T_e \hat{\mathbf{v}}_{\parallel}$. Let us multiply eq. (95) by f_e/f_{em} and integrate over velocity. This gives

$$J = - \int (f_e/f_{em}) C(f_{em}\chi) d^3\mathbf{v},$$

where J is the current carried by the electron distribution f_e . Now we utilize the self-adjointness of the linearized collision operator

$$\int \psi C(f_{em}\chi) d^3\mathbf{v} = \int \chi C(f_{em}\psi) d^3\mathbf{v},$$

together with eq. (94) for $C(f_e)$ to give

$$J = \int \mathbf{S}_w(\mathbf{v}) \cdot \nabla \chi(\mathbf{v}) d^3\mathbf{v}. \quad (96)$$

Equation (96) is the desired expression for the current. The quantity χ serves as the Green’s function for the current J . The current drive efficiency is given by

$$\frac{J}{P} = \frac{\int \mathbf{S}_w \cdot \nabla \chi d^3\mathbf{v}}{\int m_e \mathbf{S}_w \cdot \mathbf{v} d^3\mathbf{v}}. \quad (97)$$

B. Solving the adjoint equation

In order to apply this method, we must determine χ by solving eq. (95). Because $\chi(\mathbf{v})$ consists of only the first Legendre harmonic $\chi^{(1)}(v) \cos \theta$, this equation reduces to a one-dimensional integro-differential equation,

$$\frac{1}{v^2} \frac{\partial}{\partial v} v^2 D_{cvv}^{e/e} \frac{\partial \chi^{(1)}}{\partial v} - \frac{m_e v}{T_e} D_{cvv}^{e/e} \frac{\partial \chi^{(1)}}{\partial v} - \frac{2D_{c\theta\theta}^{e/e} + \Gamma^{e/e} Z_i/v}{v^2} \chi^{(1)} + I^{e/e}(\chi^{(1)}) + q_e v = 0, \quad (98)$$

where $D_{cvv}^{e/e}$ and $D_{c\theta\theta}^{e/e}$ are given by eqs. (30), and $I^{e/e}$ is defined by

$$I^{e/e}(\chi^{(1)}(v)) = \frac{C(f_{em}(v), f_{em}(v)\chi^{(1)}(v) \cos \theta)}{f_{em}(v) \cos \theta}$$

[see eq. (34)].

In general, eq. (98) must be solved numerically. This is done by constructing the partial differential equation by setting the left-hand side of eq. (98) equal to $\partial\chi^{(1)}/\partial t$. The resulting equation is integrated in time with arbitrary initial conditions until a steady state is reached. The integration is carried out in the domain $0 < v < v_{\max}$ and the boundary conditions are taken to be $\chi^{(1)}(v = 0) = 0$ and $\partial^2\chi^{(1)}(v = v_{\max})/\partial v^2 = 0$.

Approach to the steady state is accelerated by treating the first three terms in eq. (98) fully implicitly; i.e., in order to compute $[\chi^{(1)}(t + \Delta t) - \chi^{(1)}(t)]/\Delta t$, we evaluate these terms at $t + \Delta t$. This means that very large time steps can be used. The integral term $I^{e/e}(\chi^{(1)})$ is treated explicitly and is reevaluated at each time step. The resulting difference equations form a tridiagonal matrix which can be solved by Gaussian elimination.

Because the adjoint equation is the same as the equation for the perturbed distribution in the presence of a weak electric field, we can solve eq. (98) to obtain values of the electrical conductivity which is defined by

$$\frac{J}{E} = \int \frac{q_e v_{\parallel}}{T_e} f_{em}(v) \chi(\mathbf{v}) d^3\mathbf{v} = \frac{4\pi q_e}{3T_e} \int v^3 f_{em}(v) \chi^{(1)}(v) dv.$$

This procedure was carried out using the method outlined above with $v_{\max} = 15v_{te}$, $\Delta v = 0.001v_{te}$, and $\Delta t = 1000/\nu_{te}$. Because we are only working with a one-dimensional equation, it is possible to use a much finer mesh than with two-dimensional problems and so obtain results which are effectively “exact.” The results are summarized in table I where we have also included the results from use of approximate collision operators. The same technique is easily generalized to relativistic plasmas using the collision operator given in sec. X. This gives the relativistic corrections to the conductivity which are given in table II.

When the adjoint method is applied to more complicated situations (e.g., including a dc electric field), a two-dimensional equation must be solved. We can then use many of the techniques for the solution of the Fokker–Planck equation, which have been presented in the preceding sections.

C. Discussion

Let us assess the work involved in utilizing the adjoint method. Once the adjoint equation has been solved, the current and the efficiency are immediately given in terms of \mathbf{S}_w by eqs. (96) and (97). Instead of having to solve the Fokker–Planck equation afresh for every form of \mathbf{S}_w , a couple of velocity integrals over \mathbf{S}_w suffice to give the important quantities. The parameter space that must be scanned in order to give a complete understanding of the physics is greatly reduced. The adjoint method does not give the electron distribution f_e nor the rf-induced flux \mathbf{S}_w . On the other hand, a crude estimate of \mathbf{S}_w gives an accurate estimate of the efficiency because eq. (97) involves the ratio of two integrals over \mathbf{S}_w . An effective way to use this method within a ray-tracing code would be to determine \mathbf{S}_w from a solution of the one-dimensional Fokker–Planck equation¹ and to use this to determine both J and P from eqs. (96) and (20). The code thereby benefits from an accurate determination of the current drive efficiency while the high computational costs of integrating the two-dimensional Fokker–Planck equation are avoided.

Because the current drive efficiency is determined by a single function χ , it is possible to ask questions not readily answerable from numerical solutions of the Fokker–Planck equation. Examples are: What is the asymptotic form for the efficiency as the wave phase velocity becomes large? What is the maximum possible efficiency for a particular class of waves?

Besides determining the current, the adjoint method can be adapted to give other moments of the electron distribution by changing the right-hand side of eq. (XI). This can then give, for example, the perpendicular energy of the electrons, bremsstrahlung radiation, etc. This method has been used to determine the current-drive efficiency in a relativistic plasma.¹⁹ Recent developments of the method⁴² allow the determination of arbitrary moments of f_e (not just the current J), and the determination of the time development of such moments. These have been applied to the study of rf current ramp-up.⁴³

XII. Conclusions

In the last fifteen years, Fokker–Planck codes have gone from esoteric programs developed by a few researchers which could only be run on a few machines to widely available tools used by a large number of physicists on many different computers. This has been due to the large increase in computer power available to the average physicist and the pioneering efforts of Killeen *et al.*^{2,3}

In this paper, I have given a detailed description of a particular implementation of a code to solve the Fokker–Planck equation with emphasis on a particular application, namely current drive by lower hybrid waves. There are many other implementations of this code that have been applied to a large variety of interesting problems. My goal has been to illustrate the main numerical problems by means of concrete examples. The methods presented here cover the major numerical problems that are encountered in all Fokker–Planck codes.

There are two areas which still require attention. Firstly, improved methods for obtaining the steady-state solution of the Fokker–Planck equation are needed. Here the multigrid method offers the best promise for substantial savings over the other methods described in this paper. Secondly, the adjoint methods outlined in sec. XI should be extended and applied to a wider range of problems. Ray-tracing codes still need to be modified to accept the results of these calculations.

Acknowledgments

I would like to thank N. J. Fisch for a very fruitful collaboration extending over several years on various problems in rf current drive, which provided the impetus for the work described here.

This work was supported by the United States Department of Energy under Contract DE–AC02–76–CHO–3073.

Appendix A. Numerical Techniques

In this appendix, various fragments of code are shown. A two-dimensional Fokker–Planck code is ideally suited to a vector processing machine like the Cray–1. However, care must be taken to order the loops correctly, otherwise they will not vectorize.

The first example is the computation of the current $\text{int}(v \cos \theta)$ eq. (57). This illustrates the rather peculiar way in which FORTRAN code must be written in order to take advantage of the Cray–1’s architecture.⁴⁴ We assume that the arrays and variables given in table III have been initialized as indicated.

```
dimension temp(0 : iy - 1)
do 1 i = 0, iy - 1
    temp(i) = 0.0
1 continue
do 3 j = 0, jx - 1
    do 2 i = 0, iy - 1
        temp(i) = temp(i) + x(j)**3 * f(i, j)
2 continue
3 continue
do 4 i = 0, iy - 1
    temp(i) = sn(i) * cn(i) * temp(i)
4 continue
cur = 0.0
do 5 i = 0, iy - 1
```

```

    cur = cur + temp(i)
5  continue
    cur = 2.0 * pi * dx * dy * cur

```

The important point is that the inner loop (with label 2) vectorizes. This would not happen if the order of the loops were reversed. There is no particular advantage in taking the computation of $x(j)**3$ out of the inner loop since the CFT compiler does this automatically. The only loop that the compiler treats inefficiently is the last one. In fact, we replace this by a call to the OMNILIB routine `ssum`.

The second example is computing the integral part of the truncated collision operator $C(f_m(v), f^{(1)}(v) \cos \theta) / \cos \theta$ eq. (34). Here again it is easy to arrange so that most of the code vectorizes.⁴ The computation of this term is then relatively inexpensive compared with the other computations.

```

    dimension s0(-1 : jx - 1), s3(0 : jx), s5(0 : jx), f1(0 : jx - 1)
    do 1 j = 0, jx - 1
        f1(j) = 0.0
1   continue
    do 3 i = 0, iy - 1
        do 2 j = 0, jx - 1
            f1(j) = f1(j) + 1.5 * dy * sn(i) * cn(i) * f(i, j)
2   continue
3   continue
    do 4 j = 0, jx - 1
        s0(j - 1) = dx * f1(j)
        s3(j + 1) = s0(j - 1) * x(j)**3
        s5(j + 1) = s3(j + 1) * x(j)**2
4   continue
        s3(0) = 0.5 * s3(1)
        s5(0) = 0.5 * s5(1)
    do 5 j = 1, jx - 1
        s3(j) = s3(j - 1) + 0.5 * (s3(j) + s3(j + 1))
        s5(j) = s5(j - 1) + 0.5 * (s5(j) + s5(j + 1))
5   continue
        s0(jx - 1) = 0.5 * s0(jx - 2)
    do 6 j = jx - 2, 0, -1
        s0(j) = s0(j + 1) + 0.5 * (s0(j) + s0(j - 1))
6   continue
    do 7 j = 0, jx - 1
        c1(j) = (s5(j)/5.0 - s3(j)/3.0)/x(j)**2
+       + s0(j) * (x(j)**2/5.0 - 1.0/3.0) * x(j)
        c1(j) = 4 * pi * fm(j) * (f1(j) + c1(j))
7   continue

```

All the loops vectorize with the exception of the indefinite integration loops (with labels 5 and 6). Most of the time is spent in the inner loop 2 during the computation of $f^{(1)}$ eq. (15).

Finally, we consider vectorized Gaussian elimination. This subroutine performs Gaussian elimination for the tridiagonal system of equations

$$x_{i,j} + \frac{1}{2} \Delta t (a_{i,j} x_{i-1,j} + b_{i,j} x_{i,j} + c_{i,j} x_{i+1,j}) = y_{i,j},$$

to give $x_{i,j}$ for $0 \leq i < n$, $0 \leq j < m$. The coefficients satisfy $a_{0,j} = c_{n-1,j} = 0$. A substantial fraction of the running time of the Fokker–Planck code is spent in this subroutine. When implemented for a single

system of equations $m = 1$, this leads to “vector dependencies” which inhibit vectorization. The solution is to solve the m systems in parallel with j being the index for the inner loops. In the subroutine below, it is assumed that all the matrices are the same size, that the spacing in memory between $x_{i,j}$ and $x_{i+1,j}$ (the solution direction) is ns , and that the spacing between $x_{i,j}$ and $x_{i,j+1}$ (the vectorizing direction) is ms . This subroutine uses x and y as temporary storage; thus the initial data in y are destroyed.

```

subroutine solve( $x, ns, n, ms, m, a, b, c, y, dt$ )
dimension  $x(0 : ms - 1, 0 : m - 1), y(0 : ms - 1, 0 : m - 1),$ 
+           $a(0 : ms - 1, 0 : m - 1), b(0 : ms - 1, 0 : m - 1),$ 
+           $c(0 : ms - 1, 0 : m - 1)$ 
   $dt2 = 0.5 * dt$ 
  do 2  $i = 0, n - 1$ 
     $ia = ns * (i - 1)$ 
     $ib = ns * i$ 
    do 1  $j = 0, m - 1$ 
       $den = 1.0 / (1.0 + dt2 * (b(ib, j) + a(ib, j) * y(ia, j)))$ 
       $x(ib, j) = (y(ib, j) - dt2 * a(ib, j) * x(ia, j)) * den$ 
       $y(ib, j) = -dt2 * c(ib, j) * den$ 
1    continue
2  continue
  do 4  $i = n - 2, 0, -1$ 
     $ib = ns * i$ 
     $ic = ns * (i + 1)$ 
    do 3  $j = 0, m - 1$ 
       $x(ib, j) = y(ib, j) * x(ic, j) + x(ib, j)$ 
3    continue
4  continue
  return
end

```

There are a couple of tricky points here. Firstly, we use nonstandard indexing into the arrays. The element $x_{i,j}$ is accessed by the array element $x(ns * i, j)$. If $ms = 1$, then $ns * i$ will generally exceed the upper bound $ms - 1$ on the first dimension of the arrays. This type of array indexing may cause problems with compilers that perform bounds checking. Secondly, we have utilized the fact that $a(0) = c(n - 1) = 0$ and assumed that an arbitrary (possibly undefined) number multiplied by zero will give zero. If this is not the case, the $i = 0$ and $i = n - 1$ iterations in the loop with label 2 will have to be split off from the rest of the loop and treated separately.

This subroutine is sufficiently general to be used for both the matrix inversions required in implementing eq. (76). Assuming that all the matrices are dimensioned by, for example,

```

dimension  $f(0 : iyl - 1, 0 : jxl - 1)$ 

```

then the inversions are obtained by

```

call solve( $xia, iyl, jx, 1, iy, ax, bx, cx, phi, dt$ )
call solve( $xib, 1, iy, iyl, jx, ay, by, cy, xia, dt$ )

```

References

- ¹N. J. Fisch, Phys. Rev. Lett. **41**, 873 (1978).
- ²J. Killeen and K. D. Marx, in *Methods in Computational Physics*, edited by B. Alder, S. Fernback, and M. Rothenberg, volume 9, page 421, Academic, New York, 1970.
- ³J. Killeen, A. A. Mirin, and M. E. Rensink, in *Methods in Computational Physics*, edited by B. Alder, S. Fernback, and M. Rothenberg, volume 16, page 389, Academic, New York, 1976.
- ⁴M. G. McCoy, A. A. Mirin, and J. Killeen, Computer Phys. Comm. **24**, 37 (1981).
- ⁵R. M. Kulsrud, Y.-C. Sun, N. K. Winsor, and H. A. Fallon, Phys. Rev. Lett. **31**, 690 (1973).
- ⁶C. F. F. Karney and N. J. Fisch, Phys. Fluids **22**, 1817 (1979).
- ⁷T. A. Cutler, L. D. Pearlstein, and M. E. Rensink, Computation of the bounce average code, Technical Report UCRL-52233, Lawrence Livermore Laboratory, 1977.
- ⁸G. D. Kerbel and M. G. McCoy, Phys. Fluids **28**, 3629 (1985).
- ⁹Y. Matsuda and J. J. Stewart, Jr., J. Comput. Phys. **66**, 197 (1986).
- ¹⁰M. Abramowitz and I. A. Stegun, *Handbook of Mathematical Functions*, Dover, New York, 1965.
- ¹¹L. D. Landau, Phys. Z. Sowjet. **10**, 154 (1936).
- ¹²D. L. Book, *The NRL Plasma Formulary*, Naval Research Laboratory, Washington, D.C., 1983.
- ¹³M. N. Rosenbluth, W. M. MacDonald, and D. L. Judd, Phys. Rev. **107**, 1 (1957).
- ¹⁴B. A. Trubnikov, Sov. Phys. JETP. **7**, 926 (1958).
- ¹⁵B. A. Trubnikov, in *Reviews of Plasma Physics*, edited by M. A. Leontovich, volume 1, page 105, Consultants Bureau, New York, 1965.
- ¹⁶R. W. Harvey, K. D. Marx, and M. G. McCoy, Nucl. Fusion **21**, 153 (1981).
- ¹⁷S. Chapman and T. G. Cowling, *The Mathematical Theory of Non-uniform Gases*, Cambridge University Press, Cambridge, 3rd edition, 1970.
- ¹⁸S. I. Braginskii, in *Reviews of Plasma Physics*, edited by M. A. Leontovich, volume 1, page 205, Consultants Bureau, New York, 1965.
- ¹⁹C. F. F. Karney and N. J. Fisch, Phys. Fluids **28**, 116 (1985).
- ²⁰N. J. Fisch and C. F. F. Karney, Phys. Fluids **24**, 27 (1981).
- ²¹L. Spitzer and R. Härm, Phys. Rev. **89**, 977 (1953).
- ²²C. F. Kennel and F. Engelmann, Phys. Fluids **9**, 2377 (1966).
- ²³I. B. Bernstein and D. C. Baxter, Phys. Fluids **24**, 108 (1981).
- ²⁴A. Bers, in *Plasma Physics—Les Houches 1972*, edited by C. DeWitt and J. Peyraud, page 113, Gordon and Breach, New York, 1975.
- ²⁵C. F. F. Karney and N. J. Fisch, Nucl. Fusion **21**, 1549 (1981).
- ²⁶N. J. Fisch and C. F. F. Karney, Phys. Fluids **28**, 3107 (1985).
- ²⁷A. H. Kritz, K. Appert, L. Muschietti, and J. Vaclavik, in *Non-Inductive Current Drive in Tokamaks, Proc. IAEA Technical Committee Meeting, Culham, England*, edited by D. F. H. Start, volume I, page 161, 1983.
- ²⁸S. Succi, K. Appert, W. Core, H. Hamnén, T. Hellsten, and J. Vaclavik, Comp. Phys. Comm. **40**, 137 (1986).
- ²⁹V. Fuchs, M. M. Shoucri, A. Bers, and R. A. Cairns, Technical Report TV RI 187e, Institut de Recherche d'Hydro-Québec, 1985.
- ³⁰J. S. Chang and G. Cooper, J. Comput. Phys. **6**, 1 (1970).
- ³¹G. I. Marchuk, *Methods of Numerical Mathematics*, Springer-Verlag, New York, 1975.

- ³²D. W. Hewett, V. B. Krapchev, K. Hizanidis, and A. Bers, Technical Report PFC/RR-84-18, Massachusetts Institute of Technology, Plasma Fusion Center, 1984.
- ³³M. R. O'Brien, M. Cox, and D. F. H. Start, *Comp. Phys. Comm.* **40**, 123 (1986).
- ³⁴A. Brandt, *Math. Comp.* **31**, 333 (1977).
- ³⁵W. Hackbusch and U. Trottenberg, editors, *Multigrid Methods*, volume 960 of *Lecture Notes in Mathematics*, Springer-Verlag, Berlin, 1982.
- ³⁶S. T. Beliaev and G. I. Budker, *Sov. Phys. Doklady* **1**, 218 (1956).
- ³⁷S. R. de Groot, W. A. van Leeuwen, and C. G. van Weert, *Relativistic Kinetic Theory*, North-Holland, Amsterdam, 1980.
- ³⁸D. Mosher, *Phys. Fluids* **18**, 846 (1975).
- ³⁹R. A. Cairns, J. Owen, and C. N. Lashmore-Davies, *Phys. Fluids* **26**, 3475 (1983).
- ⁴⁰S. P. Hirshman, *Phys. Fluids* **23**, 1238 (1980).
- ⁴¹T. M. Antonsen, Jr. and K. R. Chu, *Phys. Fluids* **25**, 1295 (1982).
- ⁴²N. J. Fisch, *Phys. Fluids* **29**, 172 (1986).
- ⁴³C. F. F. Karney and N. J. Fisch, *Phys. Fluids* **29**, 180 (1986).
- ⁴⁴Cray Research, Inc., *CFT, the Cray-1 FORTRAN Compiler*, 1984.

Tables

TABLE I. The electrical conductivity for various values of the ion charge Z_i and for various electron-electron collision operators. The conductivities are normalized to $n_e q_e^2 / m_e \nu_{te}$.

Collision operator	$Z_i = 1$	$Z_i = 2$	$Z_i = 5$	$Z_i = 10$
linearized	7.429	4.377	2.078	1.133
drifting	6.331	3.876	1.932	1.084
Maxwellian	3.773	2.824	1.660	0.998
high-velocity	2.837	2.310	1.489	0.938

TABLE II. The electrical conductivity of a relativistic plasma for various values of the ion charge Z_i and for various electron temperatures. The conductivities are normalized to $n_e q_e^2 / m_e \nu_{te}$ and the electron temperatures are given in terms of $\Theta = T_e / m_e c^2$.

Θ	$Z_i = 1$	$Z_i = 2$	$Z_i = 5$	$Z_i = 10$
0.0	7.429	4.377	2.078	1.133
0.01	7.291	4.275	2.019	1.097
0.02	7.160	4.180	1.963	1.064
0.05	6.807	3.928	1.821	0.979
0.1	6.317	3.590	1.636	0.872
0.2	5.575	3.102	1.383	0.729

TABLE III. Meaning of FORTRAN variables and arrays.

FORTRAN name	meaning
dx	Δv
dy	$\Delta \theta$
dt	Δt
jx	N
iy	M
$xg(j)$	v_j
$x(i)$	$v_{j+1/2}$
$yg(i)$	θ_i
$y(i)$	$\theta_{i+1/2}$
$cg(i)$	$\cos \theta_i$
$cn(i)$	$\cos \theta_{i+1/2}$
$sg(i)$	$\sin \theta_i$
$sn(i)$	$\sin \theta_{i+1/2}$
pi	π
$f(i, j)$	$f_{i+1/2, j+1/2}$
$fm(j)$	$f_{m, j+1/2}$
cur	$\text{int}(v \cos \theta)$
$f1(j)$	$f^{(1)}(v_{j+1/2})$
$c1(j) * cn(i)$	$C(f_m(v), f^{(1)}(v) \cos \theta) \Big _{i+1/2, j+1/2}$
$ax(i, j)$	$a_{v, i+1/2, j+1/2}$
$ay(i, j)$	$a_{\theta, i+1/2, j+1/2}$
$phi(i, j)$	$\phi_{i+1/2, j+1/2}$

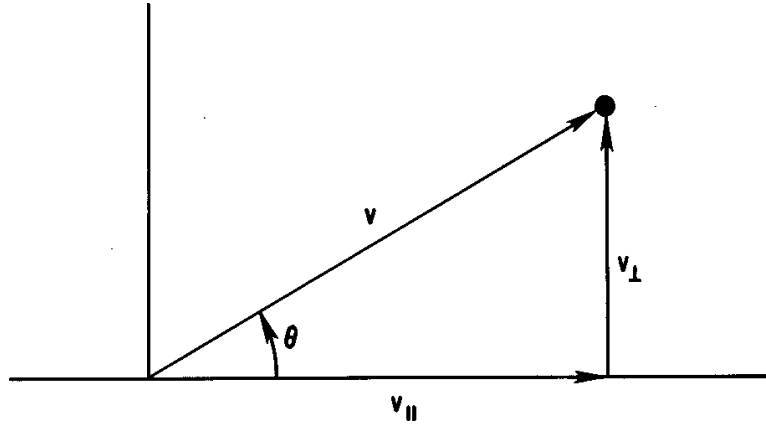


FIG. 1. The cylindrical and spherical coordinate systems.

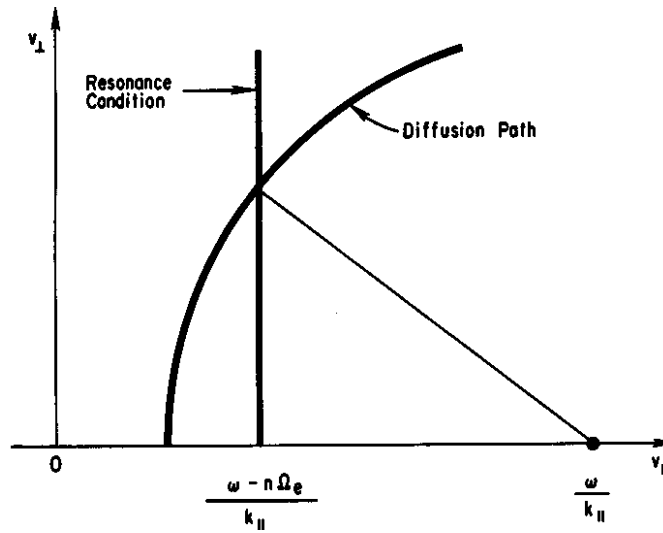


FIG. 2. The relation between the resonance condition for quasilinear diffusion $\omega - k_{\parallel}v_{\parallel} - n\Omega_e = 0$ and the diffusion path $(\mathbf{v} - (\omega/k_{\parallel})\hat{\mathbf{v}}_{\parallel})^2 = \text{const.}$

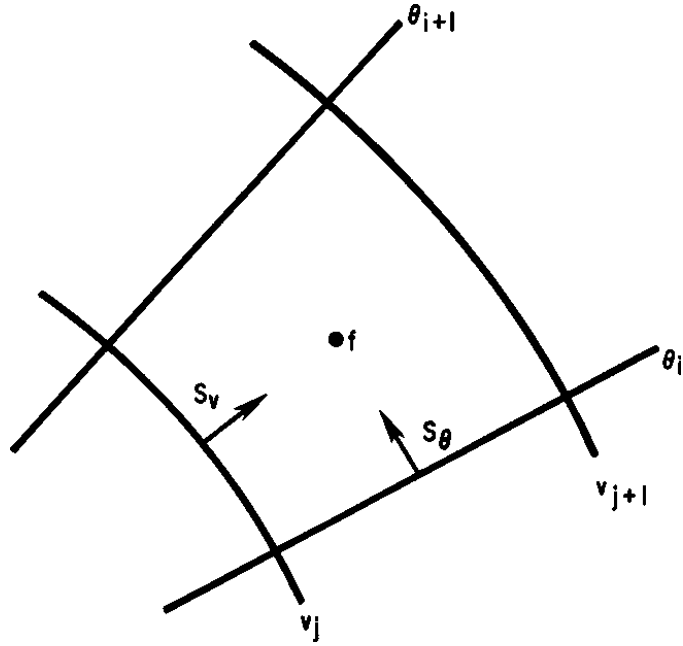


FIG. 3. The numerical grid showing where the distribution function and the fluxes are defined.

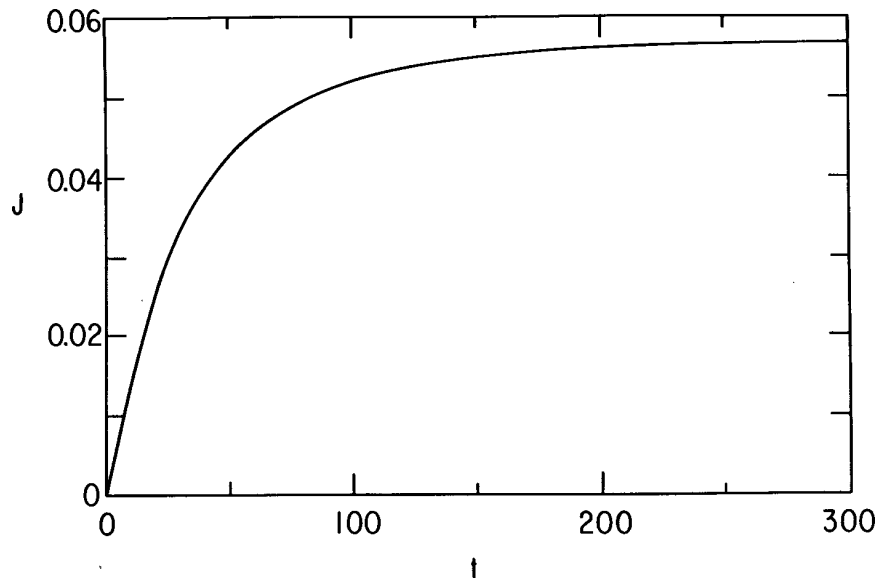


FIG. 4. The current as a function of time for $Z_i = 1$, $f(t = 0) = f_m$, and rf diffusion given by eqs. (46) with $D_0 = 1$, $v_1 = 3$, and $v_2 = 5$. Here we have $M = N = 100$, $\Delta t = 0.2$, and $v_{\max} = 10$. Electron-electron collisions are computed using $C_{\text{Max}}^{e/e}$.

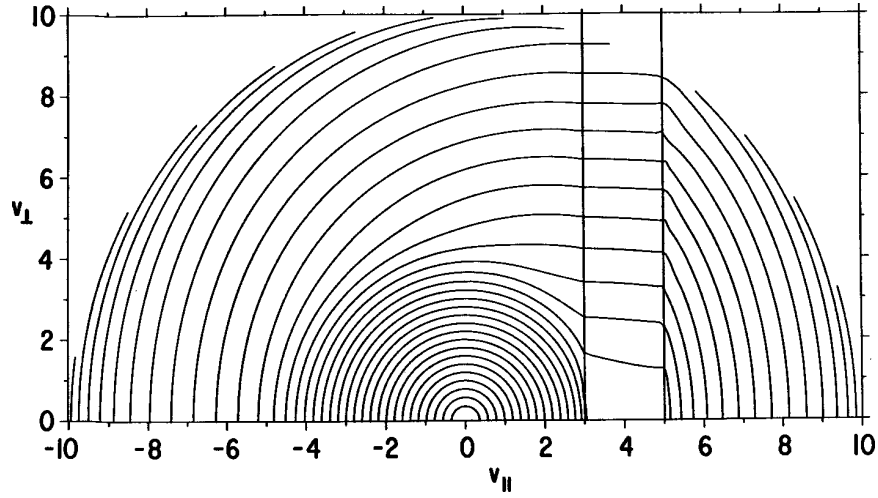


FIG. 5. The steady-state distribution for the case shown in fig. 4. The contour levels are $f = (2\pi)^{-3/2} \times \exp[-\frac{1}{2}(j/5)^2]$ for $j = \text{integer}$. This gives equally spaced contours for a Maxwellian distribution with spacing $\delta v = \frac{1}{5}$. The resonant region is shown.

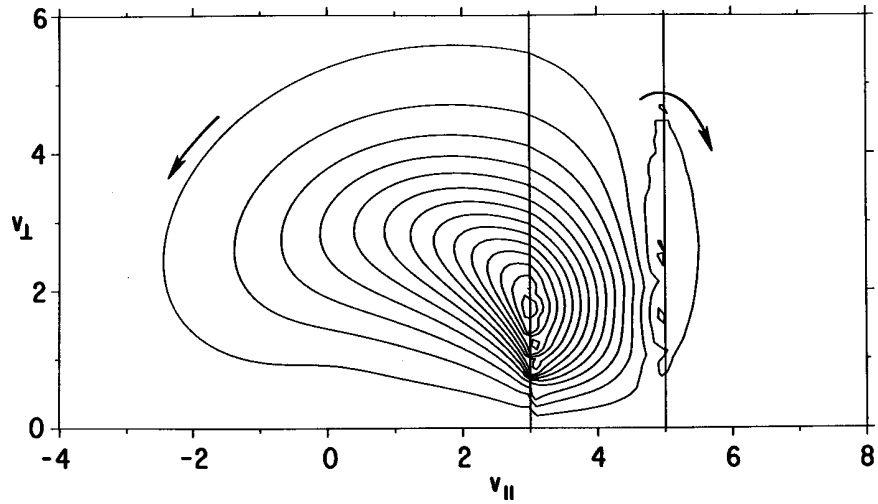


FIG. 6. The flux plot for the case shown in fig. 5. The plot was obtained by plotting contours of the stream function A , eq. (65). The contour levels are $2 \times 10^{-5}(j + \frac{1}{2})$ for $j = \text{integer}$.

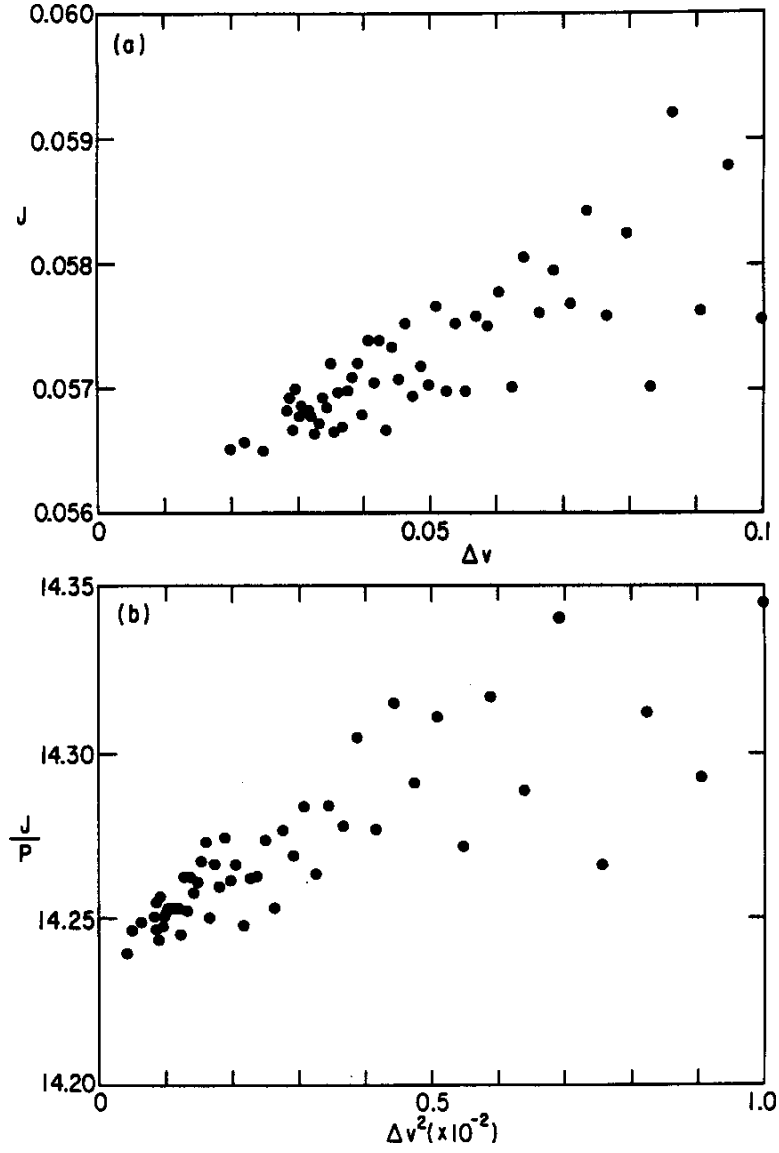


FIG. 7. The current J (a) and the efficiency J/P (b) as functions of Δv . The parameters are the same as for fig. 4 except that M and N are allowed to vary with $M = N$. The plots show the results from runs with N varying between 100 and 350 in steps of 5 and between 350 and 500 in steps of 50.

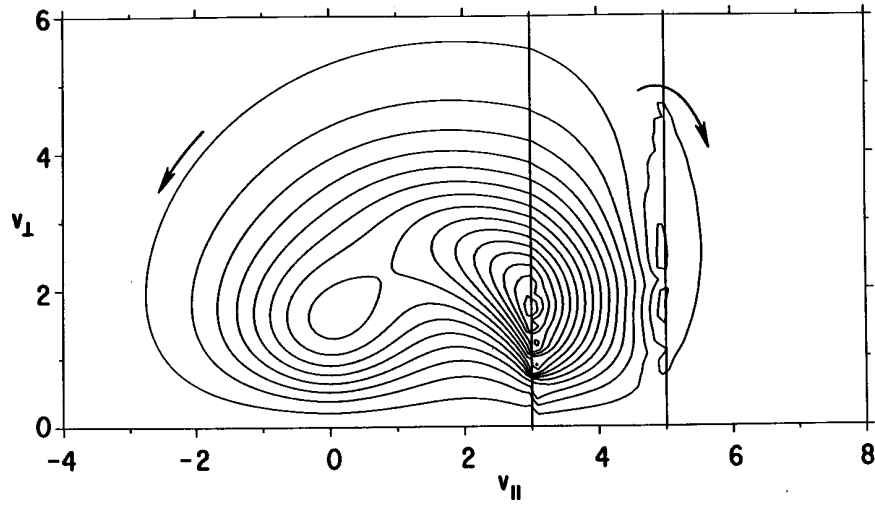


FIG. 8. The flux plot when $C_{\text{trunc}}^{e/e}$ is used. The parameters are otherwise the same as for fig. 6.

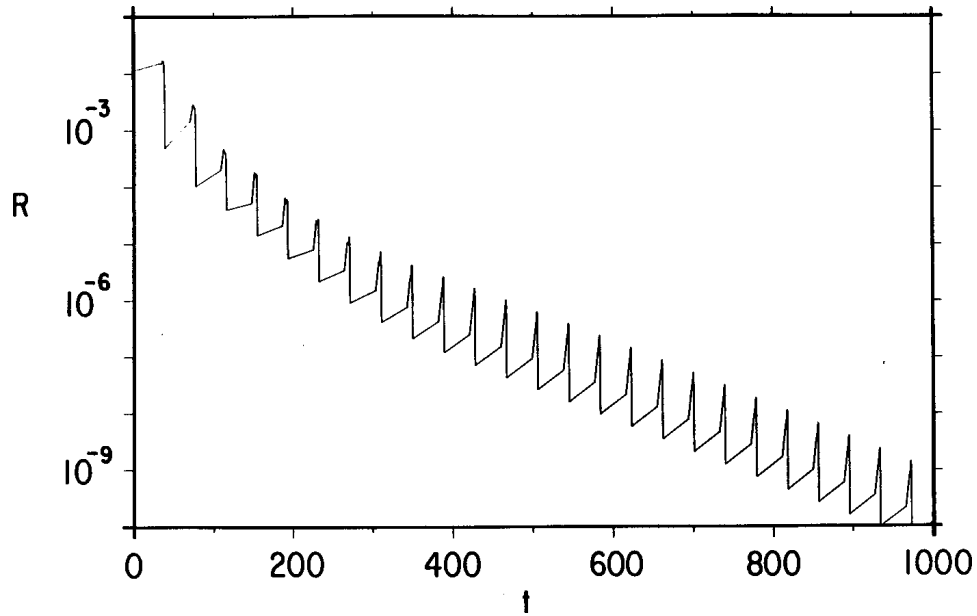


FIG. 9. R as a function of time when Chebyshev acceleration is applied to the example shown in fig. 5. Here $1/\beta = 0.05$, $1/\alpha = 1000$, $K = 20$, and $f(t = 0) = f_m$. The convergence criterion $R < 10^{-9}$ is met after 400 steps at $t = 790$.

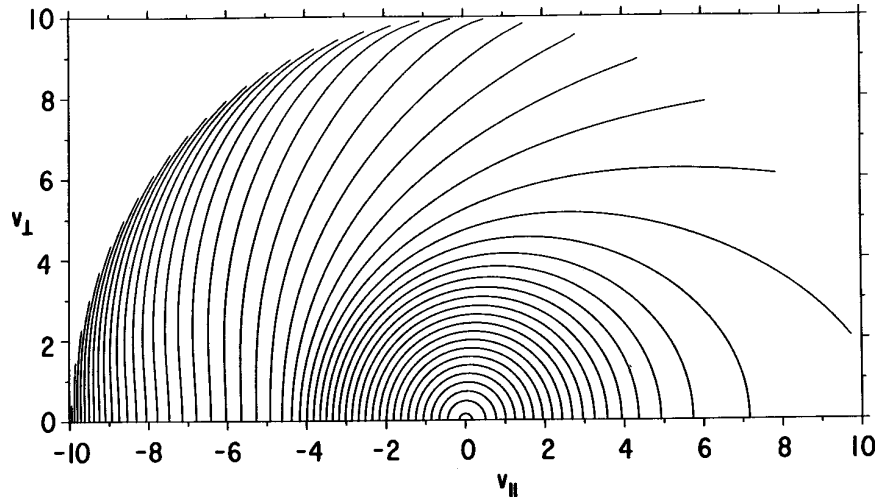


FIG. 10. The steady-state distribution in the presence of a dc electric field. Here we have $Z_i = 1$, $E = 0.06$, $M = N = 100$, $v_{\max} = 10$ and electron-electron collisions are computed using $C_{\text{Max}}^{e/e}$. The contour levels are the same as for fig. 5.

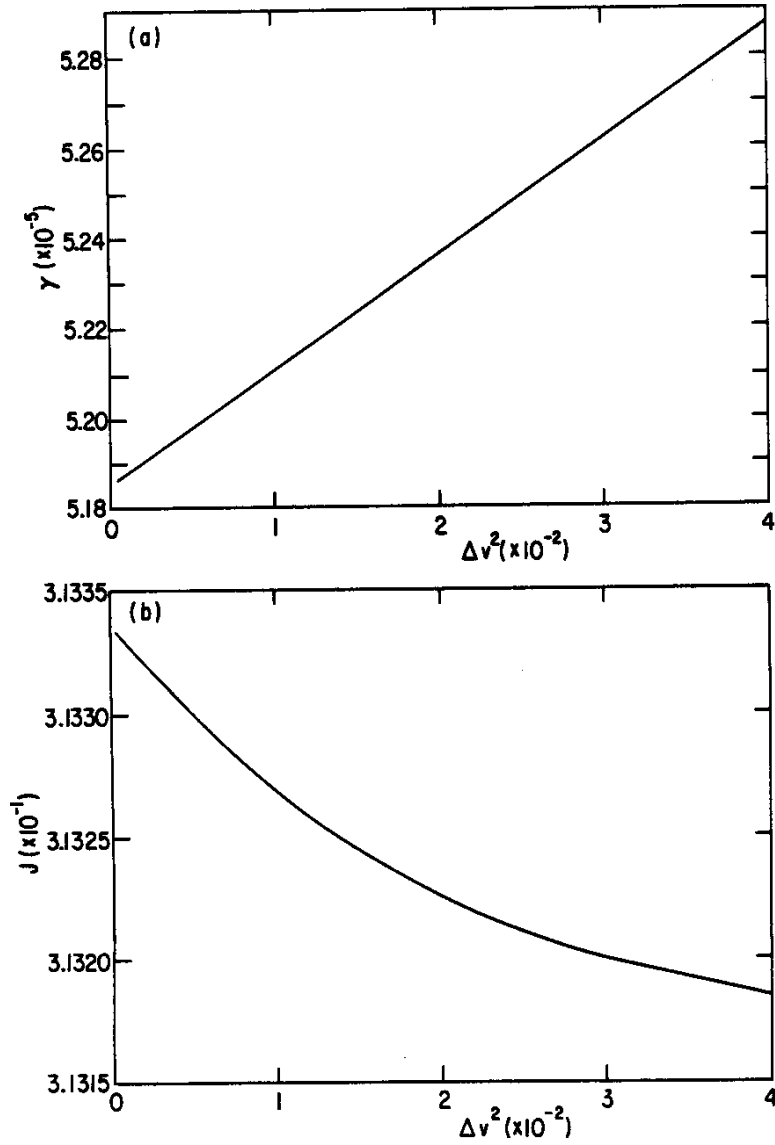


FIG. 11. The runaway rate γ (a) and the current J (b) as functions of Δv . The parameters are the same as for fig. 10 except that M and N are allowed to vary with $M = N$. The plots show the results from runs with N varying between 50 and 300 in steps of 10 and between 300 and 500 in steps of 50.

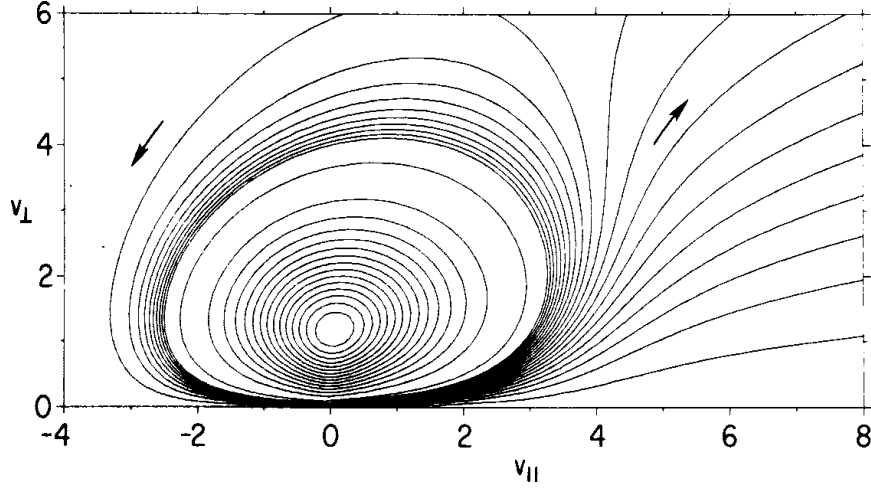


FIG. 12. The flux plot for the runaway problem. This illustrates the same case as shown in fig. 10 except that a source of particles is introduced at the origin to balance the runaway loss $\gamma = 5.148 \times 10^{-5}$. One set of contour levels is $0.1\gamma(j + \frac{1}{2})$ for $j = \text{integer}$ and $-10 \leq j < 10$ (these give the stream lines that run away and the outermost stream lines that encircle the central eddy). The other set of contour levels is $2 \times 10^{-4}(j + \frac{1}{2})$ for $j = \text{integer}$ and $j > 0$ (these are the innermost stream lines about the eddy).

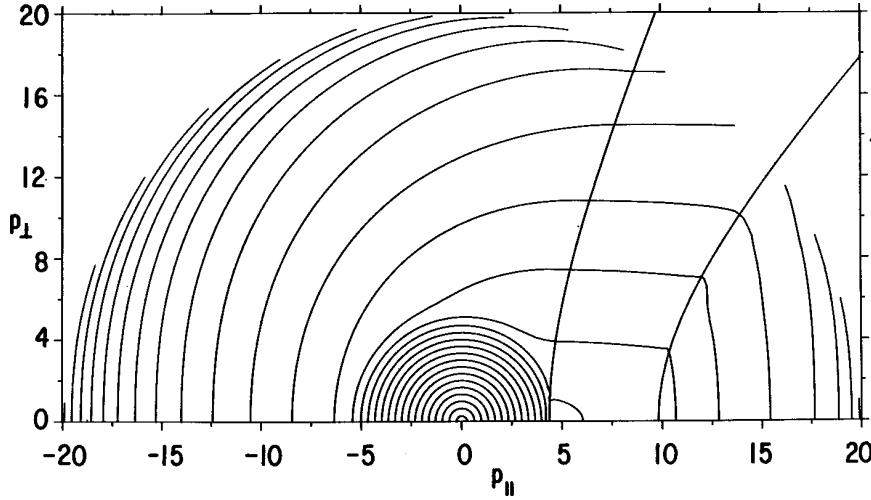


FIG. 13. The steady-state distribution for $Z_i = 1$, $\Theta = 0.01$ ($T_e = 5.11$ keV), and rf diffusion given by eq. (93) with $D_0 = 1$, $v_1 = 0.4c$, and $v_2 = 0.7c$. Here we have $M = N = 100$ and $p_{\text{max}} = 20$. Electron-electron collisions are computed using $C_{\text{trunc}}^{e/e}$. The contour levels are chosen to be $f = \sqrt{\Theta} \exp[-\sqrt{1 + \Theta(j/3)^2/\Theta}]/[4\pi K_2(\Theta^{-1})]$ for $j = \text{integer}$ which give equally spaced contours for a relativistic Maxwellian with spacing $\delta p = \frac{1}{3}$. [For $\Theta = 0.01$ we have $K_2(\Theta^{-1}) = 1.019\sqrt{\pi/2}\sqrt{\Theta} \exp(-1/\Theta)$.] The resonant region is shown.